Tutor

Dr. Joaquín F. Pérez de Benito
Departament de Ciència de Materials i Química Física

Grau de Química

Treball Final de Grau

Hexacyanoferrate(II)-hydrogen peroxide reaction: catalysis by molybdate ion

Reacció hexacianoferrat(II)-peròxid d'hidrogen: catàlisi per l'ió molibdat

Kilian Marqués Fumadó

June 2023

Universitat de Barcelona

B:KC Barcelona Knowledge Campus

No problem is too small or too trivial if we can really do something about it.

Richard Feynman

In the first place, I would like to thank Dr. Joaquín F. Pérez de Benito for letting me join him in his research project. I should also emphasize his effort to teach me the required fundamentals of chemical kinetics, and especially his accurate way to clarify all the concepts related with this topic.

Secondly, but not least, I would also like to express my gratitude to the members of my family (grandparents, mother, father and younger brother, all of them enclosed), as well as to my special and rather unique girlfriend and to my longtime friends, for their well demonstrated emotional support.

REPORT

IDENTIFICATION AND REFLECTION ON THE SUSTAINABLE DEVELOPMENT GOALS (SDG)

As we human beings certainly know, one of the things we cannot avoid is aging. This process is caused by a continuous damage of our cellular constituents throughout our lifespan, and this damage has to have a chemical nature indeed.

If we analyse more accurately those chemical injuries, we can see that one of the main contributions is the accumulative action of free radicals, specifically hydroxyl and superoxide ones. These derivate from hydrogen peroxide, which is created as an intermediate metabolite in the mitochondria of aerobic organisms: when it is reduced by transition metal ions in their lower oxidation states hydroxyl free radicals are formed, whereas when it is oxidized by transition metal ions in their higher oxidation states superoxide radicals are formed instead. Therefore, the aging process, as so many other phenomena, can be viewed as a consequence of the second law of thermodynamics: our organic compounds, being reducing in nature, are not in equilibrium with the O_2-containing atmosphere that surrounds us. Fortunately, thermodynamics does not say how much time must be elapsed for a system to reach the equilibrium state, and its evolution can be considerably slowed down.

Our work can thus belong to the third sustainable development goal (SDG), "Good Health and Well-Being" that, in turn, belongs to the area of People, given that it promotes the security and the well-being of our lives.

CONTENTS

1. SUMMARY

The reaction between hexacyanoferrate(II) ion as reducing agent and hydrogen peroxide as oxidant in slightly acidic aqueous solutions (pH 4.80 – 5.35), and in the presence of molybdate ion as catalyst, was followed by means of a spectrophotometric technique at 420 nm, wavelength at which the hexacyanoferrate(III) ion formed as a yellow product shows a maximum absorption in its visible spectrum. The catalyst was found to be very active, since a concentration as low as a thousandth part of that of hydrogen peroxide was enough to observe a notable increase in the reaction rate. The method chosen to obtain the kinetic quantitative data was that of the initial rates. This method led to non-integer kinetic orders in the three reactants for the two reaction pathways, non-catalytic and catalytic. Both paths showed acid catalysis (more appreciable in the non-catalytic one), a negative (inhibitory) saline effect and rather low activation energies (40 ± 5 kJ mol^{-1} for the non-catalytic path and 35 ± 4 kJ mol^{-1} for the catalytic one). A mechanism compatible with the available experimental information has been proposed for each reaction pathway. In the absence of molybdate ion, only the hydrated form of the reducing agent, pentacyanoaquaferrate(II) ion, is assumed to react with the oxidant, and protonation of an iron(II)-hydrogen peroxide complex leads to an internal electron transfer, yielding to the formation of a hydroxyl radical in the rate determining step. On the contrary, in the presence of catalyst, both forms of the reducing agent (hydrated and non-hydrated) are believed to react with the protonated peroxomolybdate(VI) complexes, the rate determining steps being now outer sphere electron transfer processes, yielding a molybdenum(V) complex as reaction intermediate instead of any free radical.

Keywords: hexacyanoferrate(II) ion, hydrogen peroxide, kinetics, mechanism, molybdate ion.

2. RESUM

La reacció entre l'ió hexacianoferrat(II) com agent reductor i peròxid d'hidrogen com oxidant en una solució aquosa lleugerament àcida (pH 4.80 – 5.35), i amb la presència de l'ió molibdat com a catalitzador, es va seguir mitjançant una tècnica espectrofotomètrica a 420 nm, longitud d'ona a la qual l'ió hexacianoferrat(III) format com a producte groc mostra un màxim d'absorció en el seu espectre visible. Es va trobar que el catalitzador era molt actiu, donat que a una concentració tan petita com una mil·lèsima part de la de peròxid d'hidrogen va ser suficient per observar un notable increment en la velocitat de reacció. El mètode escollit per obtenir les dades quantitatives cinètiques va ser el de les velocitats inicials. Aquest mètode ens va donar ordres cinètics no enters en els tres reactius per als dos camins de reacció, el no catalític i el catalític. Els dos camins van mostrar catàlisi àcida (més apreciable en el no catalític), un efecte salí negatiu (inhibidor) i energies d'activació bastant baixes (40 ± 5 kJ mol^{-1} per al camí de reacció no catalític i 35 ± 4 kJ mol^{-1} per al catalític). Un mecanisme compatible amb la informació experimental disponible s'ha proposat per cada camí de reacció. Amb l'absència d'ió molibdat, només la forma hidratada de l'agent reductor, l'ió pentacianoaquaferrat(II), s'assumeix que reacciona amb l'oxidant, i la protonació d'un complex de ferro(II) i peròxid d'hidrogen porta cap una transferència electrònica interna, donant lloc a la formació d'un radical hidroxil a l'etapa determinant de la velocitat. Al contrari, en presència del catalitzador, les dues formes de l'agent reductor (la hidratada i la no hidratada) es creu que reaccionen amb els complexos protonats del peroxomolibdat(VI), sent ara les etapes determinants de la velocitat processos de transferència electrònica d'esfera externa, donant lloc a un complex de molibdè(V) com a intermedi de la reacció en comptes de qualsevol radical lliure.

Paraules clau: cinètica, ió hexacianoferrat(II), ió molibdat, mecanisme, peròxid d'hidrogen.

3. INTRODUCTION

Iron(III) salts are usually water insoluble in near-neutrality media because of the precipitation of the corresponding hydroxide.[1,2] However, the addition of adequate complexing agents (such as chloride ion[3]) may reverse that insolubility. In particular, the use of hexacyanoferrate(II) and hexacyanoferrate(III) complexes is an easy and convenient way to keep iron species in aqueous solution.[4,5] Anionic ligands as cyanide ion increase the electron density on the metal center, and hence also the reducing power when found in its lower oxidation state. This can be confirmed by the values of the standard reduction potentials, E^o = 0.77 V for the $[Fe(H_2O)_6]^{3+}$ / $[Fe(H_2O)_6]^{2+}$ couple and E^o = 0.36 V for the $[Fe(CN)_6]^{3-}$ / $[Fe(CN)_6]^{4-}$ couple.[6]

On its part, hydrogen peroxide is a versatile reactant that may act either as an oxidant[7] or as a reductant,[8] depending on the chemical used as counterpart. It can even disproportionate in the presence of an adequate catalyst.[9,10] Many of the mechanisms corresponding to those processes are believed to be mediated by hydroxyl radicals formed either in the Fenton reaction[11]:

$$Fe^{2+} + H_2O_2 \longrightarrow Fe^{3+} + HO^- + HO^{\bullet} \qquad (1)$$

or in a similar process replacing iron(II) ion by another one-electron donor (Fenton-like reaction[12]):

$$Cu^{+} + H_2O_2 \longrightarrow Cu^{2+} + HO^- + HO^{\bullet} \qquad (2)$$

Moreover, hydrogen peroxide has an important biological role, coming from its being (along with the superoxide and hydroxyl radicals) one of the metabolites called reactive oxygen species (ROS).[13-15] Nevertheless, although the formation of hydroxyl radicals in the Fenton reaction (eq 1) is widely accepted in the biological field, giving rise to the well-known free radical theory of aging,[16-18] a number of chemists[19-25] has challenged this explanation, proposing the formation of an iron(IV) species instead:

$$Fe^{2+} + H_2O_2 \longrightarrow FeOH^{3+} + HO^- \qquad (3)$$

On the contrary, other authors favor formulating the Fenton reaction in its traditional way, thus leading to the formation of hydroxyl radicals.[26-31] In fact, the finding of a rather complex rate law (involving fractionary kinetic orders for the concentrations of the different chemical species) for the decomposition of hydrogen peroxide in the presence of iron(III) ion as catalyst strongly suggests a chain mechanism propagated by very reactive radical intermediates for that reaction,[32] hence tipping the scale in favor of the free radical side of the controversy.

In relation to molybdate ion, it is interesting to notice that it has been reported to be less toxic than the other analogous species (chromate and wolframate ions) belonging to the same group (6B) of the periodic table.[33,34] Actually, the three of them are known to bind hydrogen peroxide as ligand, yielding peroxochromate(VI),[35,36] peroxomolybdate(VI)[37-39] and peroxowolframate(VI)[40,41] complexes. In the case of molybdenum as the metal center, four distinct types of complexes are known, with the structures shown in Scheme 1 for their deprotonated forms.

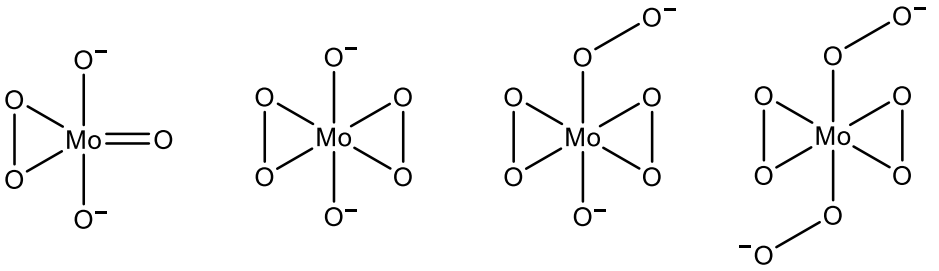

Scheme 1. Molecular structures of the mono-, di-, tri- and tetra-peroxomolybdate(VI) complexes (from left to right).

The peroxomolybdate(VI) complexes are known to show an enhanced oxidizing reactivity as compared with free hydrogen peroxide.[42,43]

On the other hand, the reaction between hexacyanoferrate ion as reducing agent and hydrogen peroxide as the oxidant in aqueous solution follows the overall stoichiometry:

$$2[Fe^{II}(CN)_6]^{4-} + H_2O_2 + 2H^+ \longrightarrow 2[Fe^{III}(CN)_6]^{3-} + 2H_2O \quad (4)$$

This redox process is believed to take place through a mechanism involving the formation of hydroxyl radicals,[44-46] and it thus closely mimics one of the main routes for the formation of those grossly harmful radicals under biological conditions.[47-49] Thus, in an attempt to search for a new route by which the biological metabolite hydrogen peroxide might decay without the intervention of free radicals in the mechanism, thus joining the action of enzymes such as catalase (catalyzing its disproportionation into water and diatomic oxygen[50]) and glutathione peroxidase (catalyzing its reduction to water[51]), a kinetic study of the catalytic effect exerted by molybdate ion on the oxidation of hexacyanoferrate ion by hydrogen peroxide (with the previous formation of intermediate mono-, di-, tri- and even tetra-peroxomolybdate complexes) might deserve some attention.

4. OBJECTIVES

In the same way that the building of a house cannot be done without having before the appropriate blueprints, the objectives to be attained should be clear at the start of a scientific project. To this purpose, we had in mind three main goals when beginning the present research:

First: *Carrying out the experimental work.* In chemical kinetics, given that the reaction rate is a function of many variables (concentrations of reactants and potential catalysts, ionic strength, pH and temperature), it is customary to perform the experiments following different series, so that only one of the conditions is changed each time. In our investigation, the variable to be tested in a determined series will be the concentration of catalyst (molybdate ion). The repetition of the series at different values of one of the other conditions will allow us to study the effect of the successive variables on the reaction rate. Since the reactant hexacyanoferrate(II) ion and all the other involved chemical species are colorless, and so transparent to the visible radiation, with the only exception of the yellow oxidation product [hexacyanoferrate(III) ion], the progress of the reaction as the latter complex accumulates in the system will be monitored with the aid of a UV-Vis spectrophotometer.

Second: *Doing the numerical calculations.* At this moment of the research, we will have some information concerning each kinetic experiment previously performed. This will consist of a list of absorbance-time couples of values obtained as the reaction advanced. The next step will be the fitting of those numerical data according to an appropriate mathematical model capable of explaining the behavior experimentally observed. The one to be tried will be an equation derived from the integrated rate law for pseudo-first order reactions, but including a time-quadratic term allowing for a certain deviation from a pseudo-first order kinetics. Then, the use of the initial rate method will lead to the kinetic parameters we are looking for. The corresponding required calculations will be implemented by means of a computer algorithm written in BASIC programming language.

Third: *Searching for a mechanistic interpretation of the macroscopic experimental data.* Indeed, a kinetic study cannot be considered as finalized until a mechanism coherent with the available experimental information can be proposed. In our case, a certain knowledge on two different reaction pathways (the non-catalytic path and the catalytic one) is expected to be attained. In particular, given the potential biological importance of this topic, it would be desirable to ascertain whether both pathways involve free radicals as reactive intermediates or it only does so the non-catalytic one.

5. EXPERIMENTAL SECTION

5.1. MATERIALS

All the experiments were done using as solvent water previously purified by deionization followed by treatment with a Millipore Synergy UV system (milli-Q quality, κ = 0.05 μS/cm at 25.0 ºC). The reactants required to carry out the redox reaction were potassium hexacyanoferrate(II) trihydrate, $K_4[Fe(CN)_6]\cdot 3H_2O$ (Merck), as the reducing agent and hydrogen peroxide, H_2O_2 (Sigma-Aldrich), as the oxidizing agent, as well as sodium molybdate dihydrate, $Na_2MoO_4\cdot 2H_2O$ (Sigma-Aldrich), as the reaction catalyst. Other chemicals used were potassium dihydrogenphosphate, KH_2PO_4 (Merck), as a source of hydrogen ions to fuel the reaction, and

both potassium chloride, KCl (Merck), and potassium nitrate, KNO_3 (Merck), to change the ionic strength of the aqueous media.

5.2. INSTRUMENTATION

The pH measurements were done by means of a Wave pH-meter, provided with a digital presentation until the second decimal figure (± 0.01 pH) and a combination electrode, calibrated with the aid of commercial buffers of known pH. The temperature was kept constant by means of a thermostatic bath Lauda E 100 also provided with a digital reading (± 0.1 ºC). The kinetic runs were followed measuring periodically the absorbances at 420 nm with a Shimadzu 160 A double beam UV-Vis spectrophotometer (± 0.001 *A*), with a thermostatted cell holder and using a quartz cell of 1 cm optical path length. At that wavelength, corresponding to violet-colored photons, the hexacyanoferrate(III) ion formed as oxidation product shows an absorption peak (ε = 1015 M^{-1} cm^{-1}),[52] yielding a yellow solution (since violet and yellow are complementary colors).

5.3. KINETIC EXPERIMENTS

The reducing agent, potassium hexacyanoferrate(II), was the last reactant to be added (1 mL of the desired concentration) to a thermostatted aqueous solution containing all the other required chemicals (24 mL), and it was prepared right before the reaction started (using to that end water previously kept at the desired temperature). The precaution of using always a fresh solution of the reductant was necessary, given that once the latter comes into contact with the solvent the hydrolyzed form of the reactant complex, a well-known intermediate of its oxidation by hydrogen peroxide,[53] starts to be formed. The total volume of the reaction mixtures was thus fixed at a constant value in all the experiments (25 mL). In order to avoid as much effect of the laboratory illumination on the reaction rate as possible, aluminum foil was used to wrap around all the glass vessels (pipette, volumetric and Erlenmeyer flasks) containing the iron(II) complex. The absorbances were periodically measured (time interval: 10 s) during 16 min (99 values). In total, 359 kinetic runs were performed.

5.4. CALCULATIONS AND GRAPHICS

The hardware used in the present work was a Hewlett-Packard personal computer, whereas the software chosen was the programming language BBC BASIC (version for Windows) for the calculations and the program KaleidaGraph (version 4.03) for the graphics.

6. DETERMINATION OF THE KINETIC DATA

In a preliminary blank experiment used as control we observed that, in the absence of hydrogen peroxide, molybdate ion did not oxidize the iron(II) complex employed in the present study as reactant. This cleared the way for us to check the activity of Mo(VI) as a potential catalyst for the oxidation of hexacyanoferrate(II) ion by hydrogen peroxide in a simple manner.

6.1. EXPERIMENTAL ABSORBANCE-TIME PLOTS

The spectrophotometer readings performed during the course of the reaction yielded all the information required for our kinetic study.

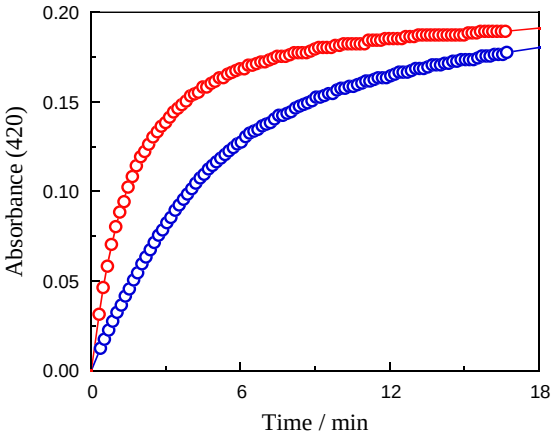

Figure 1. Absorbance at 420 nm as a function of time during the course of the reactions carried out at $[K_4Fe(CN)_6]_o = 1.97 \times 10^{-4}$ M, $[H_2O_2]_o = 7.83 \times 10^{-3}$ M, $[KH_2PO_4]_o = 1.44 \times 10^{-2}$ M, $[Na_2MoO_4]_o = 0$ (blue points) and 2.56×10^{-5} M (red points), pH 5.07 ± 0.04 and 25.0ºC.

The absorbance at 420 nm increased as the yellow product hexacyanoferrate(III) ion accumulated in the solution, but the rhythm of the evolution accelerated dramatically by a simple addition of sodium molybdate to the reaction system, demonstrating the catalytic action of the latter on the hexacyanoferrate(II) ion-hydrogen peroxide redox process (Figure 1).

The downward-concave profile of the curves reveals that the reaction rate decreased as the reaction advanced. This slowing down was caused by the decay of the concentration of the

limiting reactant, hexacyanoferrate(II) ion, since hydrogen peroxide was present in large excess (isolation method[54,55]), and it allowed us to discard the existence of autocatalysis.

As an early phase trial, we attempted to fit the absorbance-time data according to a rate law with a well-defined partial kinetic order in Fe(II). The pseudo-first order kinetic plots led to upward-concave curves, meaning that the reaction rate, both in the absence of catalyst (molybdate ion) and in its presence, decreased faster than expected for a pseudo-first order process (Figure 2, left). The pseudo-second order graphics also showed an upward-concave curvature but, given that in this case the plots were increasing (derivative > 0) instead of decreasing (derivative < 0), the meaning this time was that the reaction rate decreased more slowly than expected for a pseudo-second order process (Figure 2, right). Therefore, the conclusion to be reached was that the apparent (probably not well-defined) kinetic order of the limiting reactant was intermediary between 1 and 2.

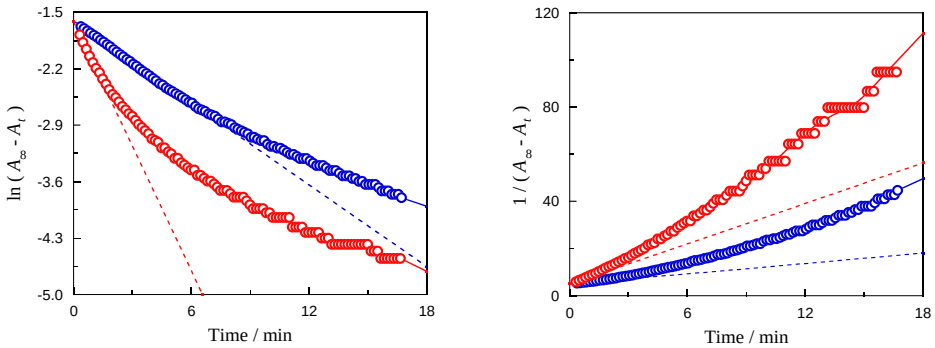

Figure 2. Attempted pseudo-first (left) and pseudo-second (right) order plots for the reactions carried out at $[K_4Fe(CN)_6]_o$ = 1.97 × 10^{-4} M, $[H_2O_2]_o$ = 7.83 × 10^{-3} M, $[KH_2PO_4]_o$ = 1.44 × 10^{-2} M, $[Na_2MoO_4]_o$ = 0 (blue points) and 2.56 × 10^{-5} M (red points), pH 5.07 ± 0.04 and 25.0ºC. The dashed lines are the tangents to the curves at t = 0.

It would indeed be desirable to specify the kinetic order associated with the limiting reactant within a narrower range of values. As can be easily demonstrated (see Appendix 1), when monitoring with the spectrophotometer the formation of a product (absorbance increasing with time), a reaction of order n would follow an integrated rate law according to which a representation of $1/(A_\infty\text{-}A_t)^{n-1}$ vs. time would lead to a linear plot. By application of a method consisting in trying different values of the kinetic order until the best linear relationship was

achieved, the results obtained were n = 1.47 for the non-catalytic reaction pathway (Figure 3, left) and n = 1.78 for the catalyzed one (Figure 3, right).

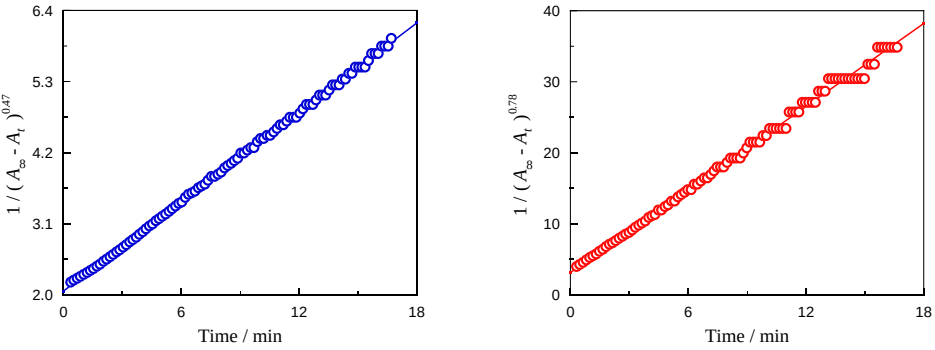

Figure 3. Pseudo-n order plots for the reactions carried out at $[K_4Fe(CN)_6]_o$ = 1.97 × 10^{-4} M, $[H_2O_2]_o$ = 7.83 × 10^{-3} M, $[KH_2PO_4]_o$ = 1.44 × 10^{-2} M, $[Na_2MoO_4]_o$ = 0 (left, n = 1.47, r = 0.9997) and 2.56 × 10^{-5} M (right, n = 1.78, r = 0.9983), pH 5.07 ± 0.04 and 25.0ºC.

Nevertheless, it should be noted that those fractionary numbers are to be considered as only apparent values, since they showed a certain dependence on the experimental conditions. Hence, it can be concluded that the reaction does not possess a well-defined kinetic order on the limiting reactant. However, some useful information can certainly be extracted from those experimental results: that the catalytic pathway slows down much faster than the non-catalytic one (given that 1.78 > 1.47), suggesting that the catalyst, Mo(VI), might be at least partially reduced to a lower oxidation state during the process, thus leading to a certain decrease in the catalytic agent concentration. Actually, it has been reported that hydrogen peroxide can completely annihilate the ubiquitous small protein cytochrome *c*, this phenomenon being most probably caused by the formation of the powerful oxidant hydroxil radical in a Fenton-like reaction, and that molybdate ion strongly inhibits the oxidative process, although in an autocatalytic-like manner, the rate increasing in a first step due to the disappearance of the inhibitor as Mo(VI) decays to a lower oxidation state.[56]

6.2. INITIAL RATE METHOD

Since, as we have just seen, the reaction had no well-defined order on the limiting reactant, and the mathematical equation governing the kinetic behavior as the redox process advances

was certainly unknown, we opted to choose the initial rate method as the best way to obtain the required quantitative information from the laboratory experiments. To that end, the first 10 points of the absorbance-time data (90 s) were fitted to:

$$\ln\ (A_\infty - A_t) \ = \ a_o \ + \ a_1\ t \ + \ a_2\ t^2 \tag{5}$$

including a time-quadratic term allowing for a certain deviation from a pseudo-first order kinetics. The rules of derivation allow us to write:

$$\frac{d[\ln\ (A_\infty - A_t)]}{dt} \ = \ a_1 \ + \ 2\ a_2\ t \tag{6}$$

$$\frac{d[\ln\ (A_\infty - A_t)]}{dt} \ = \ \frac{d[\ln\ (A_\infty - A_t)]}{d(A_\infty - A_t)}\ \frac{d(A_\infty - A_t)}{dt} \tag{7}$$

$$\frac{d[\ln\ (A_\infty - A_t)]}{dt} \ = \ -\ \frac{1}{A_\infty - A_t}\ \frac{dA_t}{dt} \tag{8}$$

$$-\ \frac{1}{A_\infty - A_t}\ \frac{dA_t}{dt} \ = \ a_1 \ + \ 2\ a_2\ t \tag{9}$$

$$\frac{dA_t}{dt} \ = \ -\ (A_\infty - A_t)\ (a_1 \ + \ 2\ a_2\ t) \tag{10}$$

$$\left(\frac{dA_t}{dt}\right)_{t\,=\,0} \ = \ -\ A_\infty\ a_1 \tag{11}$$

where it has been considered that A_o = 0 (at t = 0 the light-absorbing product has yet to be formed).

Now, according to its definition, and using the Lambert-Beer's law, the initial rate could be calculated as:

$$v_o \ = \ \frac{1}{2}\left(\frac{d\left[\mathrm{Fe(III)}\right]_t}{dt}\right)_{t\,=\,0} \ = \ \frac{1}{2\ \varepsilon_\lambda\ l}\left(\frac{dA_t}{dt}\right)_{t\,=\,0} \tag{12}$$

From eqs 11 and 12:

$$v_o = - \frac{A_\infty \, a_1}{2 \, \varepsilon_\lambda \, l} \quad (13)$$

and, since $A_\infty = \varepsilon_\lambda \, l \, c_o$:

$$v_o = - \frac{1}{2} \, a_1 \, c_o \quad (14)$$

Thus, only the second parameter of the fitting polynomial given in eq 5 is required for the calculation of the initial rate (c_o being the concentration of the limiting reactant at t = 0).

The implementation of this method for a typical experiment performed in the absence of catalyst (molybdate ion) is illustrated in Figure 4, showing the extrapolation of the absorbance-time curve and the tangent at the beginning of the reaction.

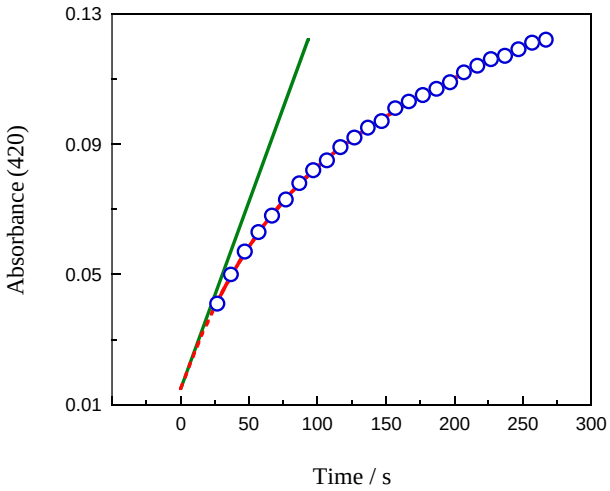

Figure 4. Absorbance at 420 nm as a function of time during the first stage of the reaction, showing the extrapolation of the curve to t = 0 (dashed line) and the tangent to the plot at that instant. $[K_4Fe(CN)_6]_o$ = 1.97×10^{-4} M, $[H_2O_2]_o$ = 1.57×10^{-2} M, $[KH_2PO_4]_o$ = 7.20×10^{-2} M, pH 4.56 and 25.0 ºC.

However, the mathematical method (eq 14) was preferred over the graphical one, because of the higher precision and readiness of implementation of the former.

7. EXPERIMENTAL KINETIC STUDY

7.1. EFFECT OF MOLYBDATE ION

Although at low initial concentrations Mo(VI) had a clear catalytic effect on the reaction (rate increasing phase), at higher concentrations a maximum followed by a rate decreasing phase were observed (Figure 5). The latter behavior could not be attributed (at least not entirely) to an inhibition effect directly provoked by molybdate ion, given that a simultaneous increase in the pH was observed right after the maximum of the bell-shaped curve, thus suggesting that the Mo(VI)-catalyzed reaction pathway might also present acid catalysis caused by hydrogen ions.

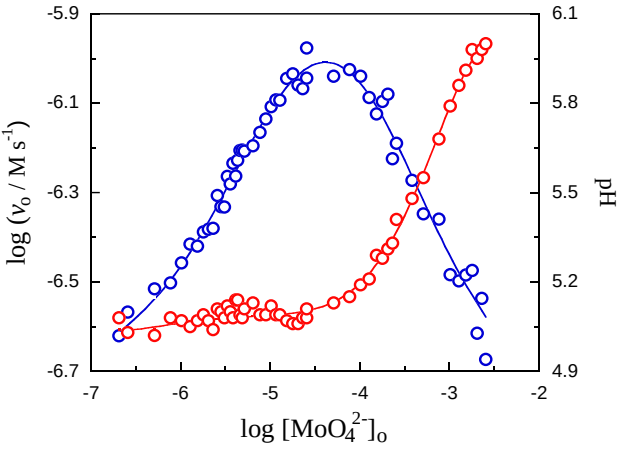

Figure 5. Logarithm of the initial rate (blue points) and pH (red points) as a function of the logarithm of the molybdate ion initial concentration at $[K_4Fe(CN)_6]_o = 1.97 \times 10^{-4}$ M, $[H_2O_2]_o = 7.83 \times 10^{-3}$ M, $[KH_2PO_4]_o = 1.44 \times 10^{-2}$ M and 25.0 ºC.

$$Mo^{VI}O_4^{2-} + xH_2O_2 \rightleftarrows [Mo^{VI}O_{4-x}(O_2)_x]^{2-} + xH_2O$$

$$[Mo^{VI}O_{4-x}(O_2)_x]^{2-} + H^+ \rightarrow [Mo^{VI}O_{3-x}(OH)(O_2)_x]^- \text{ or } [Mo^{VI}O_{4-x}(O_2)_{x-1}(O_2H)]^-$$

Scheme 2. Formation of the peroxomolybdate(VI) complexes (x = 1-4) and the subsequent protonation of either their oxy or peroxo groups.

As shown in Scheme 2, the binding of x peroxo ligands to the metal moiety requires the release of the same number of water molecules, and the increase in the pH following the addition of the catalyst could be attributed to the basicity of either molybdate ion or any of its peroxo complexes, most probably the latter (expected to be predominant in the reaction media).

An interesting enough result was that a concentration of catalyst as small as four orders of magnitude lower than that of the oxidizing agent was sufficient to notice an increase in the reaction rate, meaning that the peroxomolybdate complexes are at least one thousand times more potent as oxidants than free hydrogen peroxide.

In order to obtain the kinetic data for the experiments performed under different experimental conditions, the v_o vs. $[MoO_4^{2-}]_o$ plots were limited to the low catalyst initial concentration values, range at which a good enough linearity was achieved (Figure 6), hence following the below (first order in the catalyst) equation:

$$v_o = v_{o,nc} + k_c [MoO_4^{2-}]_o \quad (15)$$

where $v_{o,nc}$ is the initial rate of the non-catalytic reaction pathway and k_c is the pseudo-first order rate constant of the catalytic pathway.

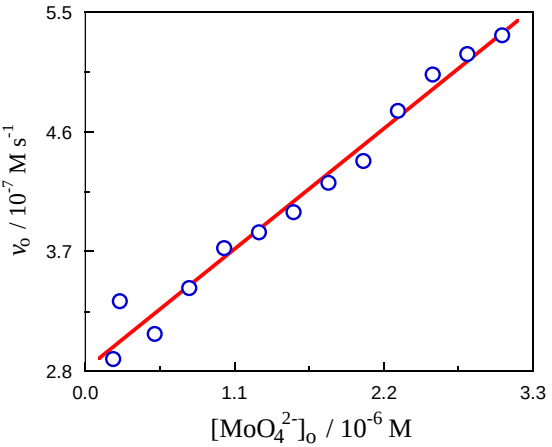

Figure 6. Initial rate as a function of the molybdate ion initial concentration at $[K_4Fe(CN)_6]_o$ = 1.97 × 10^{-4} M, $[H_2O_2]_o$ = 7.83 × 10^{-3} M, $[KH_2PO_4]_o$ = 1.44 × 10^{-2} M, pH 5.07 ± 0.03 and 25.0 ºC (r = 0.989).

Therefore, the intercept and the slope of those linear plots were able to yield some useful information on the kinetic and mechanistic nature of the non-catalytic and catalytic reaction pathways, respectively.

7.2. KINETIC DATA FROM THE EXPERIMENTAL FITS: INTERCEPTS AND SLOPES

The effect of the catalyst was studied under different experimental conditions, changing only one of the variables at a time. Then, eq 15 was used to analyze the effect of that variable on each reaction pathway separately, the information on the non-catalytic pathway being extracted from the intercept of the v_o vs. $[MoO_4^{2-}]_o$ plot and that on the catalytic one from the corresponding slope.

Rather surprisingly enough, an increase in the initial concentration of potassium hexacyanoferrate(II) led to a decrease in the value of $v_{o,nc}$, the initial rate of the non-catalytic reaction pathway (Figure 7, left), whereas that of k_c, the pseudo-first order rate constant of the catalytic pathway, remained almost invariable (Figure 7, right).

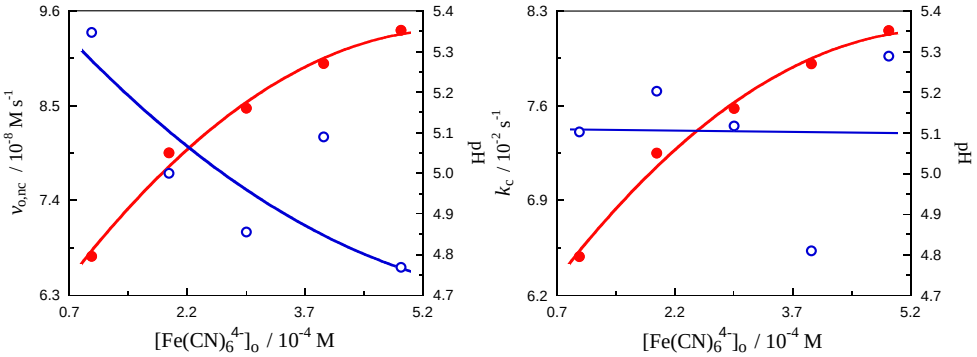

Figure 7. Initial rate of the non-catalytic reaction pathway (left, empty points), pseudo-first order rate constant of the catalytic pathway (right, empty points) and pH (filled points) as a function of the potassium hexacyanoferrate(II) initial concentration at $[H_2O_2]_o$ = 1.57 × 10^{-3} M, $[KH_2PO_4]_o$ = 1.44 × 10^{-2} M and 25.0 ºC.

At the same time, the pH of the reactant mixture increased, probably due to the protonation of the complex acting as reducing agent:

$$[Fe^{II}(CN)_6]^{4-} + H^+ \rightleftarrows [Fe^{II}(CN)_5(HCN)]^{3-} \qquad (16)$$

protonation that can be repeated in three additional steps, so that hexacyanoferrate(II) ion behaves as a quadrivalent Brönsted base.[57]

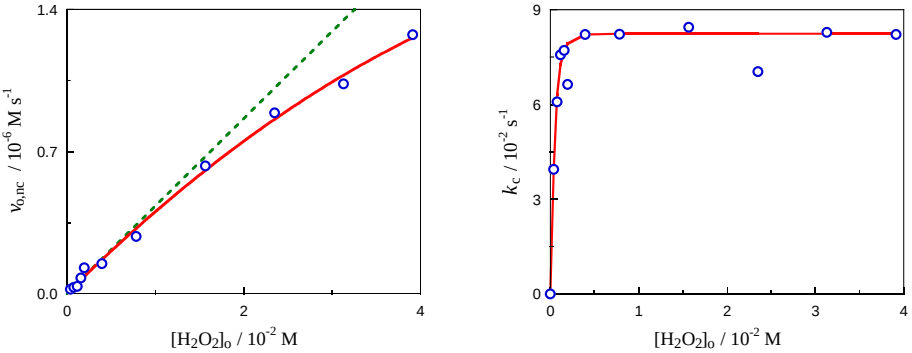

Figure 8. Initial rate of the non-catalytic reaction pathway (left) and pseudo-first order rate constant of the catalytic pathway (right) as a function of the hydrogen peroxide initial concentration at $[K_4Fe(CN)_6]_o$ = 1.97 × 10^{-4} M, $[KH_2PO_4]_o$ = 1.44 × 10^{-2} M, $[Na_2MoO_4]_o$ = (0.26 – 3.07) × 10^{-6} M, pH 5.04 ± 0.03 and 25.0 ºC. Left: the dashed line is the tangent to the plot at $[H_2O_2]_o$ = 0.

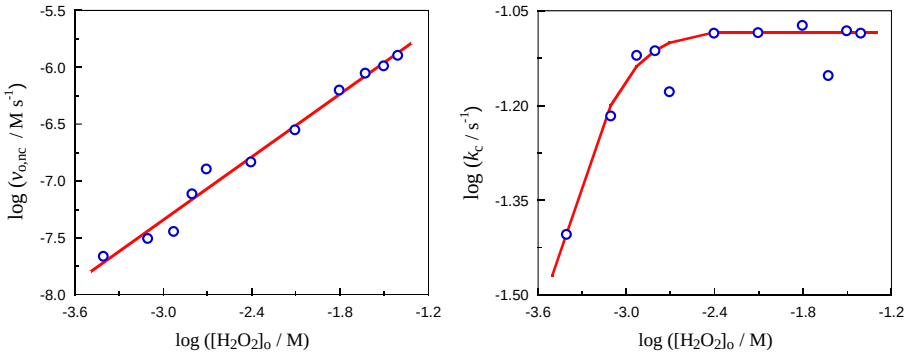

Figure 9. Double logarithmic plots of the initial rate of the non-catalytic reaction pathway (left, r = 0.9910) and pseudo-first order rate constant of the catalytic pathway (right) as a function of the hydrogen peroxide initial concentration at $[K_4Fe(CN)_6]_o$ = 1.97 × 10^{-4} M, $[KH_2PO_4]_o$ = 1.44 × 10^{-2} M, $[Na_2MoO_4]_o$ = (0.26 – 3.07) × 10^{-6} M, pH 5.04 ± 0.03 and 25.0 ºC.

The initial rate of the non-catalytic reaction pathway increased when the initial concentration of hydrogen peroxide was risen, but showing a slight downward-concave curvature (Figure 8, left). On its side, the pseudo-first order rate constant of the catalytic pathway increased in a first step, but it soon reached a plateau where the apparent order in hydrogen peroxide was close to

zero (Figure 8, right). Actually, a zero order in H_2O_2 was also found in the oxidation of iodide ion catalyzed by molybdate ion.[58]

When the graphical representations were repeated in the form of double logarithmic plots, a good linearity was observed as far as $v_{o,nc}$ was concerned (Figure 9, left), yielding a value of 0.92 ± 0.04 for the apparent (not well defined) kinetic order of H_2O_2. With respect to k_c, the new plot showed more clearly the ascending part of the curve (Figure 9, right).

When the initial concentration of potassium dihydrogen phosphate was risen, both the initial rate of the non-catalytic reaction pathway (Figure 10, left) and the pseudo-first order rate constant of the catalytic reaction pathway (Figure 10, right) increased as the pH decreased (acid catalysis). This decrease in the solution pH as the initial concentration of the phosphate component of the reactant mixture increased was caused by its acidic character:

$$H_2PO_4^- \rightleftarrows HPO_4^{2-} + H^+ \qquad (17)$$

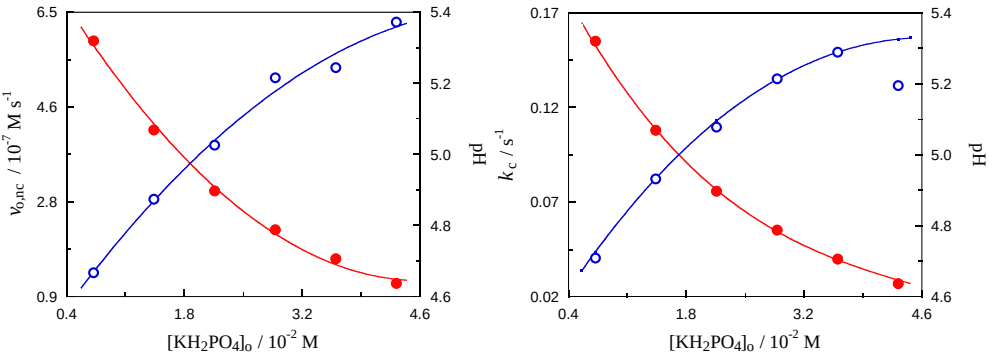

Figure 10. Initial rate of the non-catalytic reaction pathway (left, empty points), pseudo-first order rate constant of the catalytic pathway (right, empty points) and pH (filled points) as a function of the potassium dihydrogen phosphate initial concentration at $[K_4Fe(CN)_6]_o = 1.97 \times 10^{-4}$ M, $[H_2O_2]_o = 7.83 \times 10^{-3}$ M, $[Na_2MoO_4]_o = (0.20 - 3.07) \times 10^{-6}$ M and 25.0 ºC.

Addition of potassium chloride to the reaction media resulted in a decrease of both $v_{o,nc}$ (Figure 11, left) and k_c (Figure 11, right), the inhibition being more dramatic as far as the non-catalytic pathway was concerned. However, it should also be considered that the solution pH decreased simultaneously due to the action of the electrolyte (KCl) through an ionic strength effect on the equilibrium depicted in eq 17, shifting it to the right. Thus, since as pointed out

before, the reaction showed acid catalysis, the true inhibition (once discounted the accelerating contribution caused by the decreasing pH) was expected to be more intense than directly observed. This suggests that, contrary to what happens with the reaction given in eq 17, the effect on the reaction rate might be too stronger to be attributed to the ionic strength alone. Given that chloride ion is known to form stable complexes with iron(II),[59] that effect might be the result of a competition between hydrogen peroxide and chloride ion as potential ligands of the metal motif in the Fe(II) reactant complex.

In order to discriminate between the ionic strength/ligand hypotheses, and since nitrate ion behaves as a rather poor ligand,[60] although some metal-nitrate complexes are certainly known,[61] the experiments were repeated using this time KNO_3 instead of KCl as background electrolyte. As can be seen in Figure 11 (both left and right), the effects provoked by the two electrolytes on the reaction rate were quite similar, allowing us to conclude that we were standing in front of a phenomenon of ionic strength rather than one of iron(II)-anion complex formation, both chloride and nitrate essentially behaving as inert ions.

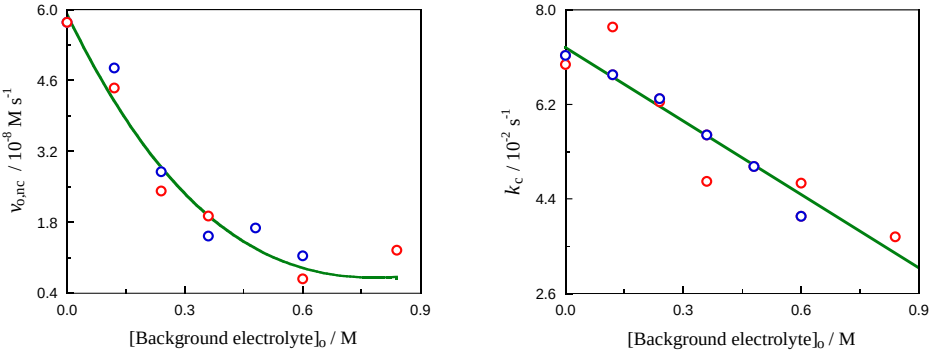

Figure 11. Initial rate of the non-catalytic reaction pathway (left) and pseudo-first order rate constant of the catalytic pathway (right, r = 0.941) as a function of the background electrolyte initial concentration (KCl: red points, KNO_3: blue points) at $[K_4Fe(CN)_6]_o = 1.97 \times 10^{-4}$ M, $[H_2O_2]_o = 1.57 \times 10^{-3}$ M, $[KH_2PO_4]_o = 1.44 \times 10^{-2}$ M, $[Na_2MoO_4]_o = (0.26 - 3.07) \times 10^{-6}$ M, pH 4.82 – 5.05 and 25.0 ºC.

Both reaction pathways followed the Arrhenius equation in the temperature range 15.0 – 35.0 ºC, yielding the activation energies 40 ± 5 kJ mol^{-1} (Figure 12, left) for the non-catalytic path and 35 ± 4 kJ mol^{-1} (Figure 12, right) for the catalytic one.

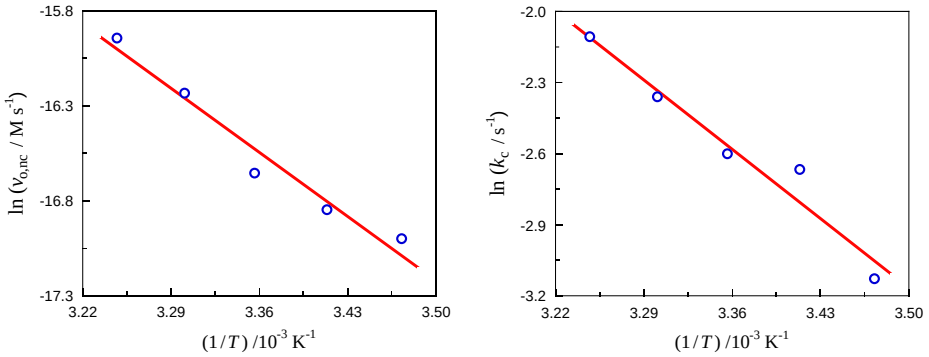

Figure 12. Arrhenius plots for the non-catalytic reaction pathway (left, r = 0.980) and the catalytic pathway (right, r = 0.977) at $[K_4Fe(CN)_6]_o$ = 1.97 × 10^{-4} M, $[H_2O_2]_o$ = 1.57 × 10^{-3} M, $[KH_2PO_4]_o$ = 1.44 × 10^{-2} M, $[Na_2MoO_4]_o$ = (0.26 – 3.07) × 10^{-6} M, pH 5.02 ± 0.03 and 15.0 – 35.0 ºC.

7.3. pH-CORRECTED KINETIC DATA

The kinetic data shown in Figure 10 at different values of the dihydrogen phosphate ion initial concentration were replotted in order to correlate them with the hydrogen ion initial concentration. Both $v_{o,nc}$ (Figure 13, left) and k_c (Figure 13, right) led to downward-concave curves, meaning that there was not a definite kinetic order in that species, the apparent order in H^+ being lower than 1 in the two cases.

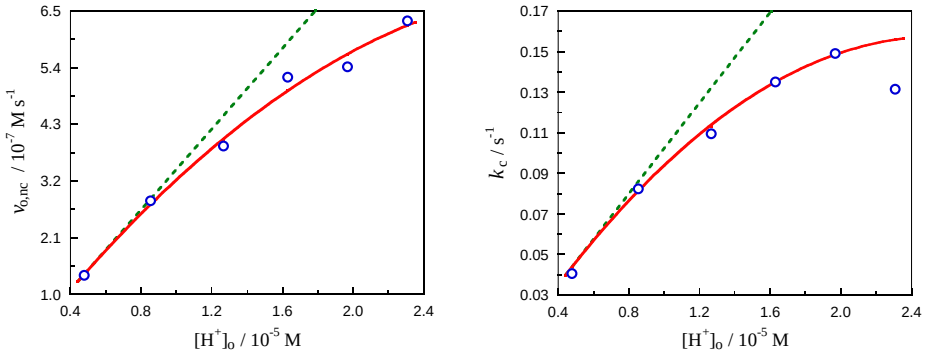

Figure 13. Initial rate of the non-catalytic reaction pathway (left) and pseudo-first order rate constant of the catalytic pathway (right) as a function of the hydrogen ion initial concentration at $[K_4Fe(CN)_6]_o$ = 1.97 × 10^{-4} M, $[H_2O_2]_o$ = 7.83 × 10^{-3} M, $[Na_2MoO_4]_o$ = (0.20 – 3.07) × 10^{-6} M, pH = 4.6 – 5.3 and 25.0 ºC. The dashed lines are the tangents to the plots at the first point.

The actual correlations found were:

$$v_{o,nc} = \frac{v_{o,nc,1}[H^+]_o}{1 + v_{o,nc,2}[H^+]_o} \quad (18)$$

$$k_c = \frac{k_{c,1}[H^+]_o}{1 + k_{c,2}[H^+]_o} \quad (19)$$

the fitting parameters being $v_{o,nc,1}$ = 3.59 × 10^{-2} s^{-1}, $v_{o,nc,2}$ = 1.36 × 10^4 M^{-1}, $k_{c,1}$ = 1.22 × 10^4 M^{-1} s^{-1} and $k_{c,2}$ = 3.07 × 10^4 M^{-1}.

The mathematical formulas given in eqs 18 and 19 were proven to be useful to correct the kinetic parameters in those places where necessary. Both the $v_{o,nc}$ vs. $[Fe(CN)_6^{4-}]_o$ (Figure 14, left) and k_c vs. $[Fe(CN)_6^{4-}]_o$ (Figure 14, right) pH-corrected plots showed a downward concave curvature, hence demonstrating that the kinetic order of the reducing agent was not well defined in any of the reaction pathways, the apparent value being again in the 0 – 1 range.

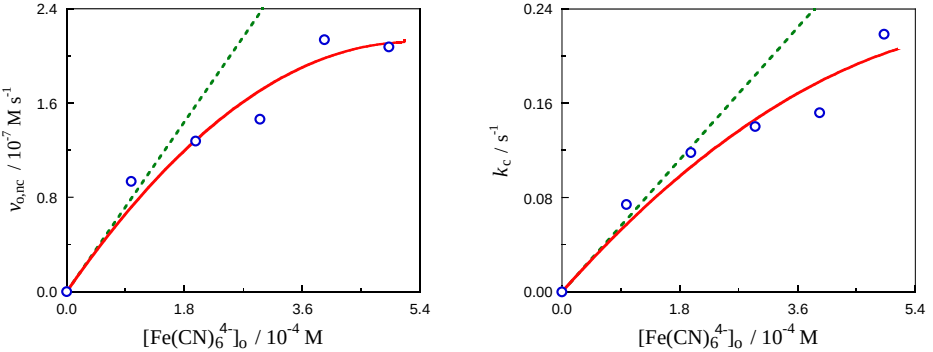

Figure 14. Initial rate of the non-catalytic reaction pathway (left) and pseudo-first order rate constant of the catalytic pathway (right) as a function of the potassium hexacyanoferrate(II) initial concentration at $[H_2O_2]_o$ = 1.57 × 10^{-3} M, $[KH_2PO_4]_o$ = 1.44 × 10^{-2} M, pH 4.80 – 5.35 and 25.0 ºC. The experimental values were corrected and referred to a constant pH (4.80). The dashed lines are the tangents to the plots at $[K_4Fe(CN)_6]_o$ = 0.

Actually, double logarithmic plots led to the slopes 0.53 ± 0.08 (Figure 15, left) and 0.61 ± 0.08 (Figure 15, right) for the non-catalytic and catalytic pathways, respectively.

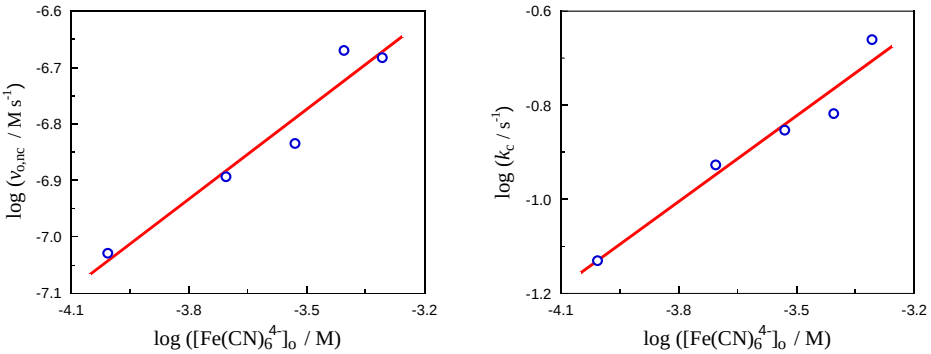

Figure 15. Double logarithmic plots of the initial rate of the non-catalytic reaction pathway (left) and pseudo-first order rate constant of the catalytic pathway (right) as a function of the potassium hexacyanoferrate(II) initial concentration at $[K_4Fe(CN)_6]_o = (0.98 - 4.92) \times 10^{-4}$ M, $[H_2O_2]_o = 1.57 \times 10^{-3}$ M, $[KH_2PO_4]_o = 1.44 \times 10^{-2}$ M, pH 4.80 – 5.35 and 25.0 ºC. The experimental values were corrected and referred to a constant pH (4.80).

7.4. APPARENT KINETIC ORDERS OF THE REACTANTS

Once corrected the experimental data where necessary, the use of double logarithmic plots allowed to obtain the kinetic orders of the three reactants for the two involved reaction pathways (apparent values at least). The results, compiled in Table 1, indicated that the six of them were non-integer (fractional) numbers, although the partial kinetic orders of both hydrogen peroxide and hydrogen ion in the non-catalytic pathway were very close to unity.

Reaction pathway	Order (Fe^{II})	Order (H_2O_2)	Order (H^+)
Non-catalytic	0.53 ± 0.08	0.92 ± 0.04	0.96 ± 0.06
Catalytic	0.61 ± 0.08	– 0.02 ± 0.04	0.80 ± 0.12

(a) The value for hydrogen peroxide in the catalytic reaction pathway is referred to the plateau observed at $[H_2O_2]_o \geq 3.94 \times 10^{-3}$ M.

Table 1. Kinetic orders of the reactants (apparent values).

7.5. HOW MUCH IRON(II) HAS REACTED VIA EACH REACTION PATHWAY?

Certainly, this question is difficult to answer in an exact way, but at least we can try to find an approximate solution. First of all, let us start by assuming that both the non-catalytic and catalytic reaction pathways are of about the same apparent order (α) in the limiting reactant,

Fe(II), and that the Mo(VI) acting as catalyst is regenerated in the mechanism, not being reduced to a lower oxidation state at the end of the process.

Based on these assumptions, the concentration of Fe(II) that has reacted through each pathway during the whole reaction can be calculated as:

$$(\Delta c)_{nc} = \int_0^{c_o} \frac{k_{nc,\alpha}\, c^{\alpha}}{k_{nc,\alpha}\, c^{\alpha} + k_{c,1+\alpha}\, c^{\alpha}\, [Mo^{VI}]_o}\, dc \qquad (20)$$

$$(\Delta c)_{c} = \int_0^{c_o} \frac{k_{c,1+\alpha}\, c^{\alpha}\, [Mo^{VI}]_o}{k_{nc,\alpha}\, c^{\alpha} + k_{c,1+\alpha}\, c^{\alpha}\, [Mo^{VI}]_o}\, dc \qquad (21)$$

where c_o and c are the concentrations of the limiting reactant at times 0 and t, respectively, $k_{nc,\alpha}$ the pseudo-rate constant of order α associated with the non-catalytic reaction pathway and $k_{c,1+\alpha}$ the pseudo-rate constant of order $1+\alpha$ associated with the catalytic pathway. The involved integral is immediate, leading for the concentration of Fe(II) reacted through the non-catalytic pathway:

$$(\Delta c)_{nc} = \frac{k_{nc,\alpha}\, c_o}{k_{nc,\alpha} + k_{c,1+\alpha}\, [Mo^{VI}]_o} \qquad (22)$$

and for the catalytic pathway:

$$(\Delta c)_{c} = \frac{k_{c,1+\alpha}\, [Mo^{VI}]_o\, c_o}{k_{nc,\alpha} + k_{c,1+\alpha}\, [Mo^{VI}]_o} \qquad (23)$$

Application of eqs 22 and 23 to the kinetic data shown in Figures 8 and 14 allowed to determine the percentage contribution corresponding to each reaction pathway. The results indicated that the initial concentration of the reducing agent, Fe(II), had a negligible effect on those relative contributions (Table 2), being within the laboratory error margin (see Appendix 2 for the statistical treatment of experimental errors).

$[Fe(CN)_6^{4-}]_o$ [10^{-4} M]	$(PC)_{nc}$ [%]	$(PC)_c$ [%]
0.98	29 ± 4	71 ± 4
1.97	26 ± 2	74 ± 2
2.95	25 ± 6	75 ± 6
3.94	31 ± 7	69 ± 7
4.92	24 ± 6	76 ± 6

(a) $(PC)_{nc}$ stands for the percentage contribution of the non-catalytic pathway to the overall reaction.
(b) $(PC)_c$ stands for the percentage contribution of the catalytic pathway to the overall reaction.

Table 2. Percentage contributions of the non-catalytic and catalytic reaction pathways at different potassium hexacyanoferrate(II) initial concentrations. $[H_2O_2]_o = 1.57 \times 10^{-3}$ M, $[KH_2PO_4]_o = 1.44 \times 10^{-2}$ M, pH 4.80 (fixed) and 25.0ºC.

On the contrary, the initial concentration of the oxidizing agent, H_2O_2, had a notable effect on the percentage attributable to each pathway, that corresponding to the catalytic path decreasing dramatically as $[H_2O_2]_o$ increased (Figure 16).

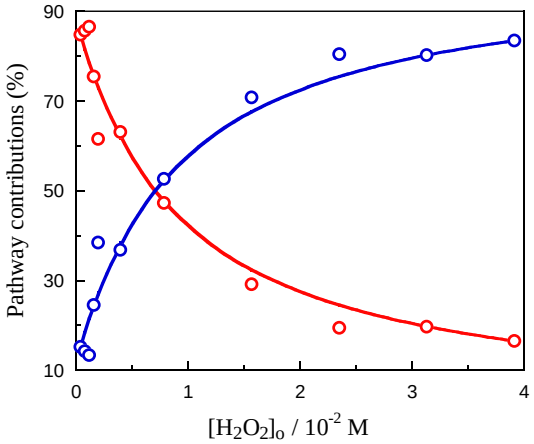

Figure 16. Percentage contributions of the non-catalytic (blue points) and catalytic (red points) reaction pathways as a function of the initial concentration of the oxidizing agent at $[K_4Fe(CN)_6]_o = 1.97 \times 10^{-4}$ M, $[KH_2PO_4]_o = 1.44 \times 10^{-2}$ M, $[Na_2MoO_4]_o = (0.26 - 3.07) \times 10^{-6}$ M, pH 5.04 ± 0.03 and 25.0 ºC.

8. MICROSCOPIC INTERPRETATION

Now, the moment has arrived when the macroscopic information obtained from the laboratory measurements should shed some light on the microscopic aspects underlying the kinetic data.

8.1. MECHANISM: NON-CATALYTIC REACTION PATHWAY

For the molybdate-independent reaction pathway, the following mechanism can be proposed:

$$[Fe^{II}(CN)_6]^{4-} + H_2O \underset{}{\overset{K_1}{\rightleftharpoons}} [Fe^{II}(CN)_5(H_2O)]^{3-} + CN^- \quad (24)$$

$$[Fe^{II}(CN)_5(H_2O)]^{3-} + H_2O_2 \overset{K_2}{\rightleftharpoons} [Fe^{II}(CN)_5(H_2O_2)]^{3-} + H_2O \quad (25)$$

$$[Fe^{II}(CN)_5(H_2O_2)]^{3-} + H^+ \overset{K_3}{\rightleftharpoons} [Fe^{II}(CN)_5(H_3O_2)]^{2-} \quad (26)$$

$$[Fe^{II}(CN)_5(H_3O_2)]^{2-} \xrightarrow[\text{slow}]{k_4} [Fe^{III}(CN)_5(H_2O)]^{2-} + HO^{\bullet} \quad (27)$$

$$HO^{\bullet} + [Fe^{II}(CN)_6]^{4-} \xrightarrow{k_5} HO^- + [Fe^{III}(CN)_6]^{3-} \quad (28)$$

The proposed mechanism for this pathway starts with the hydrolysis of the initial complex acting as one of the reactants to yield pentacyanoaquaferrate(II) ion (eq 24). This species has been found to be the active intermediate in the oxidation of hexacyanoferrate(II) ion by hydrogen peroxide.[62] Moreover, a similar requirement has been reported for the reaction between cisplatin (a well-known antitumoral agent[63]) and thiols, where the replacement of a chloride ligand by a water molecule precedes the binding of the sulfur-containing substrate with the metal atom.[64] In the next step, eq 25, the hydrogen peroxide molecule enters the first-coordination sphere of the iron(II) center. Protonation of the peroxide ligand in eq 26 decreases its electron density, thus enhancing its oxidizing power, so that an inner-sphere electron transfer from the metal to the protonated ligand can take place in the slow step (eq 27, Scheme 3),

yielding as an intermediate a hydroxyl radical with an exacerbated reactivity capable of oxidizing a second hexacyanoferrate(II) ion (eq 28).

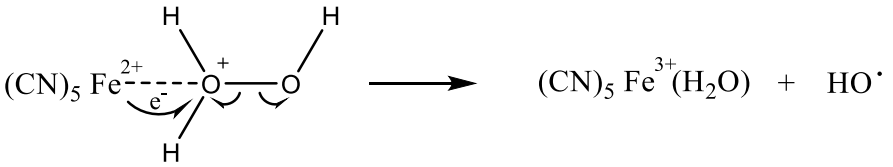

Scheme 3. Inner-sphere electron transfer in the rate determining step of the non-catalytic reaction pathway.

8.2. MECHANISM: CATALYTIC REACTION PATHWAY

In the case of the molybdate-dependent reaction pathway, the following mechanism can be proposed for a generic peroxomolybdate complex with x peroxo ligands acting as the oxidizing agent:

$$HMo^{VI}O_4^- + xH_2O_2 \xrightleftharpoons{K_6} H[Mo^{VI}O_{4-x}(O_2)_x]^- + xH_2O \quad (29)$$

$$H[Mo^{VI}O_{4-x}(O_2)_x]^- + H^+ \xrightleftharpoons{K_7} H_2[Mo^{VI}O_{4-x}(O_2)_x] \quad (30)$$

$$[Fe^{II}(CN)_6]^{4-} + H_2[Mo^{VI}O_{4-x}(O_2)_x] \xrightarrow[\text{slow}]{k_8} [Fe^{III}(CN)_6]^{3-} + H_2[Mo^{V}O_{4-x}(O_2)_x]^- \quad (31)$$

$$[Fe^{II}(CN)_5(H_2O)]^{3-} + H_2[Mo^{VI}O_{4-x}(O_2)_x] \xrightarrow[\text{slow}]{k_9} [Fe^{III}(CN)_5(H_2O)]^{2-} + H_2[Mo^{V}O_{4-x}(O_2)_x]^- \quad (32)$$

$$2H_2[Mo^{V}O_{4-x}(O_2)_x]^- \xrightarrow{k_{10}} H_2[Mo^{VI}O_{4-x}(O_2)_x] + H_2[Mo^{IV}O_{4-x}(O_2)_x]^{2-} \quad (33)$$

$$H_2[Mo^{IV}O_{4-x}(O_2)_x]^{2-} \xrightarrow{k_{11}} [Mo^{VI}O_{5-x}(O_2)_{x-1}]^{2-} + H_2O \quad (34)$$

In the first step (eq 29), we have proposed the formation of the four different peroxomolybdate complexes (x = 1 – 4) as the active forms of the catalyst. In the second step (eq 30), a protonation of those complexes takes place, thus decreasing their electron density and once again enhancing their oxidizing power. We have also proposed the split of the catalytic pathway into two other smaller pathways, each with its own slow step (the first redox elementary reaction within each pathway). Although in the case of the non-catalytic pathway we have suggested the participation of an inner-sphere electron transfer (eq 27), we have preferred in this case another kind of mechanism, namely an outer-sphere electron transfer,[65-67] involving either hexacyanoferrate(II) ion (eq 31) or its hydrated form (eq 32) and leading to a molybdenum(V) peroxo complex intermediate in both cases. The mechanism ends with two fast steps: the dismutation of Mo(V) into Mo(VI) and Mo(IV) (eq 33), and a posterior internal redox process within the latter, thus regenerating the Mo(VI) catalyst (eq 34).

8.3. RATE LAW: NON-CATALYTIC REACTION PATHWAY

In order to find the kinetic rate law that can be inferred from the mechanism proposed for the non-catalytic reaction pathway, it is necessary to eliminate the concentrations of all the intermediates involved in the sequence of elementary reactions. This end will be attained by applying two mathematical approximations: the quasi-equilibrium hypothesis to the reversible fast steps (eqs 24-26) and the steady state hypothesis to the hydroxyl free radical formed in the slow step (eq 27) as a low-concentration, very reactive intermediate.[68]

Given the overall stoichiometry of the reaction (see eq 4), we can define the rate as:

$$v = \frac{1}{2}\frac{d[Fe^{III}]}{dt} \quad (35)$$

and taking into consideration that the product iron(III) is formed in eqs 27 and 28:

$$v_{nc} = \frac{1}{2}(v_4 + v_5) \quad (36)$$

Now, applying the steady state approximation to the hydroxyl radical:

$$\frac{d[HO^{\bullet}]}{dt} = v_4 - v_5 = 0 \quad (37)$$

$$v_5 = v_4 \quad (38)$$

and carrying this result into eq 36:

$$v_{nc} = v_4 = k_4 [Fe^{II}(CN)_5(H_3O_2)^{2-}] \quad (39)$$

The concentration of the complex intermediate of iron(II) with protonated hydrogen peroxide can be eliminated by applying this time the quasi-equilibrium approximation to eq 26:

$$K_3 = \frac{[Fe^{II}(CN)_5(H_3O_2)^{2-}]}{[Fe^{II}(CN)_5(H_2O_2)^{3-}][H^+]} \quad (40)$$

In addition, a simple matter balance allows to write:

$$[Fe^{II}(CN)_5(H_2O_2)^{3-}]_T = [Fe^{II}(CN)_5(H_2O_2)^{3-}] + [Fe^{II}(CN)_5(H_3O_2)^{2-}] \quad (41)$$

so that eqs 40 and 41 lead to:

$$[Fe^{II}(CN)_5(H_3O_2)^{2-}] = \frac{K_3 [Fe^{II}(CN)_5(H_2O_2)^{3-}]_T [H^+]}{1 + K_3 [H^+]} \quad (42)$$

or approximately:

$$[Fe^{II}(CN)_5(H_3O_2)^{2-}] = \frac{K_3 [Fe^{II}(CN)_5(H_2O_2)^{3-}] [H^+]}{1 + K_3 [H^+]} \quad (43)$$

where it has been considered that $[Fe^{II}(CN)_5(H_3O_2)^{2-}] << [Fe^{II}(CN)_5(H_2O_2)^{3-}]$, that is to say, that the protonated form of the iron(II)-hydrogen peroxide complex is present in minute concentration. Carrying this result into eq 39:

$$v_{nc} = \frac{K_3 k_4 [Fe^{II}(CN)_5(H_2O_2)^{3-}][H^+]}{1 + K_3 [H^+]} \quad (44)$$

This mathematical procedure can be repeated this time for the quasi-equilibrium depicted in eq 25, leading to:

$$[Fe^{II}(CN)_5(H_2O_2)^{3-}] = \frac{K_2 [Fe^{II}(CN)_5(H_2O)^{3-}][H_2O_2]}{1 + K_2 [H_2O_2]} \quad (45)$$

$$v_{nc} = \frac{K_2 K_3 k_4 [Fe^{II}(CN)_5(H_2O)^{3-}][H_2O_2][H^+]}{(1 + K_2 [H_2O_2])(1 + K_3 [H^+])} \quad (46)$$

From the quasi-equilibrium approximation applied to eq 24 it follows that:

$$K_1 = \frac{[Fe^{II}(CN)_5(H_2O)^{3-}][CN^-]}{[Fe^{II}(CN)_6{}^{4-}]} \quad (47)$$

but, since all the available experimental information obtained in the laboratory is referred to the initial reaction rate and, since at t = 0 the concentrations of pentacyanoaquaferrate(II) and cyanide ions are equal, we can write:

$$[Fe^{II}(CN)_5(H_2O)^{3-}]_o = \left(K_1 [Fe^{II}(CN)_6{}^{4-}]_o\right)^{\frac{1}{2}} \quad (48)$$

and along with eq 46, we finally obtain:

$$v_{o,nc} = \frac{K_1^{1/2} K_2 K_3 k_4 [Fe^{II}(CN)_6{}^{4-}]_o{}^{1/2} [H_2O_2]_o [H^+]_o}{(1 + K_2 [H_2O_2]_o)(1 + K_3 [H^+]_o)} \quad (49)$$

8.4. RATE LAW: CATALYTIC REACTION PATHWAY

Given that the rate monitoring species was iron(III) and that, as far as the catalytic pathway is concerned, this reaction product is formed in eqs 31 and 32, we have that:

$$v_c = \frac{1}{2}(v_8 + v_9) \quad (50)$$

where:

$$v_8 = k_8 [Fe^{II}(CN)_6^{4-}] [H_2Mo^{VI}O_{4-x}(O_2)_x] \quad (51)$$

$$v_9 = k_9 [Fe^{II}(CN)_5(H_2O)^{3-}] [H_2Mo^{VI}O_{4-x}(O_2)_x] \quad (52)$$

The concentration of the molybdenum intermediate involved in eqs 51 and 52 can be deduced from the application of the quasi-equilibrium approximation to the step shown in eq 30:

$$K_7 = \frac{[H_2Mo^{VI}O_{4-x}(O_2)_x]}{[HMo^{VI}O_{4-x}(O_2)_x^-] [H^+]} \quad (53)$$

and from eqs 48 and 50-53, we finally arrive at:

$$v_{o,c} = \frac{K_7 k_S [HMo^{VI}O_{4-x}(O_2)_x^-]_o [H^+]_o}{2 (1 + K_7 [H^+]_o)} \quad (54)$$

where:

$$k_S = k_8 [Fe^{II}(CN)_6^{4-}]_o + K_1^{1/2} k_9 [Fe^{II}(CN)_6^{4-}]_o^{1/2} \quad (55)$$

The relationships between the concentrations of the different peroxo complexes and the initial concentrations of both molybdate ion and hydrogen peroxide are deduced in Appendix 3.

8.5. CONTRASTING WITH THE MACROSCOPIC EXPERIMENTAL INFORMATION

Equation 49 is consistent with the dependence of the initial rate of the non-catalytic reaction pathway on the initial concentration of hexacyanoferrate(II) ion (theoretical order 0.50 vs. experimental value 0.53 ± 0.08). It is also consistent with the dependence on the initial concentration of hydrogen peroxide: whereas a double logarithmic plot led to an apparent kinetic order with the experimental value 0.92 ± 0.04, a non-linear least square fit of $v_{o,nc}$ vs. $[H_2O_2]_o$ led to K_2 = 11.9 M^{-1}. Moreover, a comparison of the experimental dependence of $v_{o,nc}$ vs. $[H^+]_o$ (eq 18) with its theoretical counterpart (eq 49) led to K_3 = 1.36 × 10^4 M^{-1}. The inhibitory effect of the ionic strength on the initial rate of the non-catalytic reaction pathway

(negative saline effect) suggests the involvement of a reaction anion-cation in the mechanism, in concordance with eq 26.

On the other hand, eqs 54 and 55 are also coherent with the dependences of the initial rate of the catalytic reaction pathway on the initial concentrations of the three reactants. According to the proposed mechanism, the apparent kinetic order of hexacyanoferrate(II) ion should be intermediary between 0.5 and 1, the experimental value being 0.61 ± 0.08. With respect to the dependence on the initial concentration of hydrogen peroxide, the fast increase of parameter k_C at low values of $[H_2O_2]_o$ corresponds to the formation of the peroxomolybdate complexes, whereas the plateau observed at high values of $[H_2O_2]_o$ corresponds to a situation where the complexation has already been completed (see Figure 8, right). As far as the dependence on the initial concentration of hydrogen ion is concerned, a comparison of the experimental correlation (eq 19) with the theoretical version (eq 54) led to the value $K_7 = 3.07 \times 10^4$ M^{-1}. In addition, the rate law inferred from the mechanism proposed for the catalytic pathway leads to a first-order dependence on the initial concentration of molybdenum(VI), in concordance with the experimental findings (eq 15). Again, the observation of a negative saline effect as far as the catalytic reaction pathway is concerned agrees well with a reaction anion-cation (eq 30).

9. CONCLUSIONS

(i) The redox reaction between hexacynoferrate(II) ion and hydrogen peroxide in slightly acidic aqueous solutions (pH 4.80 – 5.35), both in the absence and presence of molybdate ion as catalyst, exhibited a complex behavior, showing a clear-cut deviation from either pseudo-first or pseudo-second order kinetics, even under a large excess of the oxidant.

(ii) The initial rate method was the one preferred to obtain the quantitative kinetic information on the reaction.

(iii) The initial rate showed a first-order dependence on the molybdate ion initial concentration, and the intercept and slope of the corresponding linear plots yielded some useful kinetic information on the non-catalytic and catalytic reaction pathways, respectively.

(iv) Non-integer kinetic orders (some of them not well defined) in the three reactants (oxidizing agent, reducing agent and hydrogen ion) were found for the two reaction pathways.

(v) Both pathways showed acid catalysis, so that a decrease in the solution pH led to an increase in the rate of each reaction path, the increase being more intense for the non-catalytic one.

(vi) An increase in the ionic strength led to a decrease in the reaction rate (inhibitory saline effect), the same observation again in the two pathways, but again more intense in the case of the non-catalytic path.

(vii) Both reaction pathways followed the Arrhenius equation in the temperature range 15.0 – 35.0 ºC, yielding an activation energy of 40 ± 5 kJ mol^{-1} for the non-catalytic path and slightly lower, 35 ± 4 kJ mol^{-1}, for the catalytic one.

(viii) The mechanisms proposed for the two reaction pathways are consistent with the non-integer (fractional) kinetic orders found for the three reactants. The one corresponding to the non-catalytic path assumes that only the hydrated form of the iron(II) complex is active enough to react with hydrogen peroxide, and that a hydroxyl radical is formed in the rate determining step, whereas that proposed for the catalytic path assumes that both forms of the iron(II) complex (hydrated and non-hydrated) can react with the peroxomolybdate(VI) complexes, and that no free radicals are involved as intermediates.

10. REFERENCES

1. Baltpurvins, K. A; Burns, R. C; Lawrance, G. A; Stuart, A. D. Effect of Ca^{2+}, Mg^{2+}, and Anion Type on the Aging of Iron(III) Hydroxide Precipitates. *Environ. Sci. Techol.* **1997**, *31*, 1024-1032.
2. Bogoczek, R.; Kociolek-Balawejder, E.; Stanislawska, E.; Zabska, A. Using Macroporous N-Chlorosulfonamide S/DVB Copolymer as an Aid to Iron Removal from Water. *Pure Appl. Chem.* **2007**, *79*, 1491-1503.
3. Liu, X. W.; Millero, F. J. The Solubility of Iron Hydroxide in Sodium Chloride Solutions. *Geochim. Cosmochim. Acta* **1999**, *61*, 3487-3497.
4. Meeussen, J. C. L.; Keizer, M. G.; Dehaan, F. A. M. Chemical-stability and Decomposition Rate of Iron Cyanide Complexes in Soil Solution. *Environ. Sci. Tech.* **1992**, *26*, 511-516.
5. Ghosh, R. S.; Murarka, I. P.; Nakles, D.V.; Neuhauser, E. F. Refinement of Weak Acid Dissociable (WAD) Method for Measuring Weak Metal Cyanide Complexes in Aqueous Samples. *Environ. Eng. Scil.* **2005**, *22*, 543-556.
6. Edwards, J. O.; Curci, R. In *Catalytic Oxidation with Hydrogen Peroxide as Oxidant*; Strukul, G., Ed.; Kluwer: Dordrecht, 1992.
7. Gurwitsch, A. A.; Eremeyev, V. F.; Karabchievsky, Y. A. Ultra-weak Emission in Visible and Ultra-violet Regions in Oxidation of Solutions of Glycine by Hydrogen Peroxide. *Nature* **1965**, *206*, 20-22.
8. Yuan, F.; Yan, J.; Yu, W.; Du, J.; Yu, J. Nitric Oxide Reduction by Hydrogen Peroxide Absorption through a Ceramic Hollow Fiber Membrane Contactor. *J. Environ. Chem. Eng.* **2020**, *8*, 104129.
9. Perez-Benito, J. F. Reaction Pathways in the Decomposition of Hydrogen Peroxide Catalyzed by Copper(II). *J. Inorg. Biochem.* **2004**, *98*, 430-438.
10. Batabyal, M.; Upadhyay, A.; Kadu, R.; Birudukota, N. C.; Chopra, D.; Kumar, S. Tetravalent Spiroselenurane Catalysts: Intramolecular Se···N Chalcogen Bond-driven Catalytic Disproportionation of H_2O_2 to H_2O and O_2 and Activation of I_2 and NBS. *Inorg. Chem.* **2022**, *61*, 8729-8745.
11. Ni, W.; Jiang, K.; Ke, Q.; Su, J.; Cao, X.; Zhang, L.; Li, C. Development of an Intelligent Heterojunction Fenton Catalyst for Chemodynamic/starvation Synergistic Cancer Therapy. *J. Mater. Sci. Technol.* **2023**, *141*, 11-20.
12. Han, M.; Wang, H.; Jin, W.; Chu, W.; Xu, Z. The Performance and Mechanism of Iron-Mediated Chemical Oxidation: Advances in Hydrogen Peroxide, Persulfate and Percarbonate Oxidation. *J. Environ. Sci.* **2022**, *128*, 181-202.
13. Sun, H.; Xu, J.; Wang, Y.; Shen, S.; Xu, X.; Zhang, L.; Jiang, Q. Bone Microenvironment Regulative Hydrogels with ROS Scavenging and Prolonged Oxygen-generating for Enhancing Bone Repair. *Bioact. Mater.* **2023**, *24*, 477-496.
14. Wang, L.; Liu, C.; Lu, W.; Xu, L.; Kuang, L.; Hua, D. ROS-sensitive Crocin-loaded Chitosan Microspheres for Lung Targeting and Attenuation of Radiation-induced Lung Injury. *Carbohydr. Polym.* **2023**, *307*, 120628.
15. Yan, H.; Chen, H.; Zhao, J.; Yao, T.; Ding, X. Postharvest H_2O_2 Treatment Affects Flavor Quality, Texture Quality and ROS Metabolism of 'Hongshi' Kiwifruit Fruit Kept at Ambient Conditions. *Food Chem.* **2023**, *405*, 134908.
16. Son, J. M.; Lee, C. Aging: All Roads Lead to Mitochondria. *Semin. Cell Dev. Biol.* **2021**, *116*, 160-168.
17. Park, S.; Kim, B. K.; Park, S. K. Effects of Fisetin, a Plant-Derived Flavonoid, on Response to Oxidative Stress, Aging, and Age-Related Diseases in *Caenorhabditis elegans*. *Pharmaceuticals* **2022**, *15*, 1528.
18. Polidori, M. C.; Mecocci, P. Modeling the Dynamics of Energy Imbalance: the Free Radical Theory of Aging and Frailty Revisited. *Free Radic. Biol. Med.* **2022**, *181*, 235-240.
19. Sawyer, D. T.; Kang, C.; Llobet, A.; Redman, C. Fenton Reagents (1:1 $Fe^{II}L_x$/HOOH) React via $[L_xFe^{II}OOH(BH^+)]$ as Hydroxylases (RH → ROH), Not as Generators of Free Hydroxyl Radicals ($HO^·$). *J. Am. Chem. Soc.* **1993**, *115*, 5817-5818.

20. Hage, J. P.; Llobet, A.; Sawyer, D. T. Aromatic Hydroxylation by Fenton Reagents {Reactive Intermediate [$L_x{}^+Fe^{III}OOH(BH^+)$], Not Free Hydroxyl Radical ($HO^·$)}. *Bioorg. Med. Chem.* **1995**, *3*, 1383-1388.
21. Sawyer, D. T.; Sobkowiak, A.; Matsushita, T. Metal [ML_x; M = Fe, Cu, Co, Mn]/Hydroperoxide-Induced Activation of Dioxygen for the Oxygenation of Hydrocarbons: Oxygenated Fenton Chemistry. *Acc. Chem. Res.* **1996**, *29*, 409-416.
22. Rachmilovich-Calis, S.; Masarwa, A.; Meyerstein, N.; Meyerstein, D. The Fenton Reaction in Aerated Aqueous Solutions Revisited. *Eur. J. Inorg. Chem.* **2005**, 2875-2880.
23. Kremer, M. L. Strong Inhibition of the Fe^{3+}+ H_2O_2 Reaction by Ethanol: Evidence against the Free Radical Theory. *Prog. React. Kinet. Mech.* **2017**, *42*, 397-413.
24. Kremer, M. L. New Kinetic Analysis of the Fenton Reaction: Critical Examination of the Free Radical-Chain Reaction Concept. *Prog. React. Kinet. Mech.* **2019**, *44*, 289-299.
25. Kremer, M. L. Initial Steps in the Reaction of H_2O_2 with Fe^{2+} and Fe^{3+} Ions: Inconsistency in the Free Radical Theory. *Reactions* **2023**, *4*, 171-175.
26. Walling, C. Intermediates in the Reactions of Fenton Type Reagents. *Acc. Chem. Res.* **1998**, *31*, 155-157.
27. Marusawa, H.; Ichikawa, K.; Narita, N.; Murakami, H.; Ito, K.; Tezuka, T. Hydroxyl Radical as a Strong Electrophilic Species. *Bioorg. Med. Chem.* **2002**, *10*, 2283-2290.
28. Perez-Benito, J. F. Reaction Pathways in the Decomposition of Hydrogen Peroxide Catalyzed by Copper(II). *J. Inorg. Biochem.* **2004**, *98*, 430-438.
29. Zeng, Q.; Wang, X.; Liu, X.; Huang, L.; Hu, J.; Chu, R.; Tolic, N.; Dong, H. Mutual Interactions between Reduced Fe-Bearing Clay Minerals and Humic Acids under Dark, Oxygenated Conditions: Hydroxyl Radical Generation and Humic Acid Transformation. *Environ. Sci. Technol.* **2020**, *54*, 15013-15023.
30. Sun, X.; Gu, X.; Lyu, S. The Performance of Chlorobenzene Degradation in Groundwater: Comparison of Hydrogen Peroxide, Nanoscale Calcium Peroxide and Sodium Percarbonate Activated with Ferrous Iron. *Water Sci. Technol.* **2021**, *83*, 344-357.
31. Chen, H.; Fang, C.; Gao, X.; Jiang, G.; Wang, X.; Sun, S.; Wu, W.; Wu, Z. Sintering- and Oxidation-Resistant Ultrasmall Cu(I)/(II) Oxides Supported on Defect-Rich Mesoporous Alumina Microspheres Boosting Catalytic Ozonation. *J. Colloid Interface Sci.* **2021**, *581*, 964-978.
32. Perez-Benito, J. F. Iron(III)-Hydrogen Peroxide Reaction: Kinetic Evidence of a Hydroxyl-Mediated Chain Mechanism. *J. Phys. Chem. A* **2004**, *108*, 4853-4858.
33. Fairhall, L. T.; Dunn, R. C.; Sharpless, N. E.; Pritchard, E. A. The Toxicity of Molybdenum. *Publ. Health Bull.* **1945**, *293*, 1-36.
34. Budavari, S. (Ed.) *The Merck Index*; Merck: Rahway, New Jersey, 1989.
35. Miesel, R.; Kurpisz, M.; Kroger, H. Suppression of Inflammatory Arthritis by Simultaneous Inhibition of Nitric Oxide Synthase and NADPH Oxidase. *Free Radic. Biol. Med.* **1996**, *20*, 75-81.
36. Perez-Benito, J. F.; Arias, C. A Kinetic Study of the Chromium(VI)-Hydrogen Peroxide Reaction. Role of the Diperoxochromate(VI) Intermediates. *J. Phys. Chem. A* **1997**, *101*, 4726-4733.
37. Csanyi, L. J. On the Peroxomolybdate Complexes as Sources of Singlet Oxygen. *J. Mol. Catal. A* **2010**, *322*, 1-6.
38. Ciszewski, M; Benke, G; Leszczynska-Sejda, K; Kopyto, D. Facile Synthesis of Reduced Graphene Oxide/Peroxomolybdate(VI)-Citrate Composite and its Potential Energy Storage Application. *Appl. Phys. A* **2017**, *123*, 713.
39. Amitouche, D.; Haouas, M.; Mazari, T.; Mouanni, S.; Canioni, R.; Rabia, C.; Cadot, E.; Marchal-Roch, C. The Primary Stages of Polyoxomolybdate Catalyzed Cyclohexanone Oxidation by Hydrogen Peroxide as Investigated by *in situ* NMR. Substrate Activation and Evolution of the Working Catalyst. *Appl. Catal. A* **2018**, *561*, 104-116.

40. Qi, Z.; Li, H.; Chen, J.; Ye, C.; Qiu, T. Intensification of Oxidative Desulfurization by Zr(IV)-Ionic Liquid-HPW Composite Activating H_2O_2 System and Mechanism Insight. *Fuel* **2022**, *322*, 124231.
41. Zhang, Z.; He, T.; Qi, Y.; Dai, Y.; Lao, K.; Gou, X. Rapid and Highly Specific Detection of Site-specific 5-Hydroxymethylcytosine Based on Peroxotungstate Oxidation and Mismatch Ligation-based Lamp. *RSC Adv.* **2022**, *12*, 19885-19889.
42. Srinivasan, S.; Ford, W. T. Epoxidation of Ciclooctene with Aqueous Hydrogen Peroxide Catalyzed by Molybdate Bound to Colloidal Polymers. *New J. Chem.* **1991**, *15*, 693-699.
43. Boruah, J. J.; Ahmed, K.; Das, S.; Gogoi, S. R.; Saikia, G.; Sharma, M.; Islam, N. S. Peroxomolybdate Supported on Water Soluble Polymers as Efficient Catalysts for Green and Selective Sulfoxidation in Aqueous Medium. *J. Mol. Catal. A* **2016**, *425*, 21-30.
44. Malhotra, S.; Agarwai, R.; Saini, S. K. Photo-oxidation of Hexacyanoferrate(II) and (III) Ions in Aqueous Solution. *Indian J. Chem. A* **1998**, *37*, 830-833.
45. Laszlo, Z.; Dombi, A. Oxidation of $[Fe(CN)_6]^{4-}$ and Reduction of $[Fe(CN)_6]^{3-}$ by VUV-irradiated Aqueous Solutions. *Chemosphere* **2002**, *46*, 491-494.
46. Perez-Benito, J. F.; Pages-Rebull, J. Oxidation of Hexacyanoferrate(II) Ion by Hydrogen Peroxide: Evidence of Free Radical Intermediacy. *React. Kinet. Mech. Catal.* **2021**, *133,* 631-653.
47. Jacobson, E. S. Pathogenic Roles for Fungal Melanins. *Clin. Microbiol. Rev.* **2000**, *13*, 708-717.
48. Suh, M.; Keasey, S. L.; Brueggemann, E. E.; Ulrich, R. G. Antibiotic-dependent Perturbations of Extended Spectrum *beta*-Lactamase Producing Klebsiella Pneumoniae Proteome. *Proteomics.* **2017**, *17*, 1700003.
49. Ning, Y.; Huo, Y.; Xue, H.; Du, Y.; Yao, Y.; Sedgwick, A. C.; Lin, H.; Li, C.; Jiang, S.; Wang, B.; Gao, S.; Kang, L.; Sessler, J. L.; Zhang, J. Tri-Manganese(III) Salen-Based Cryptands: A Metal Cooperative Antioxidant Strategy that Overcomes Ischemic Stroke Damage *in vivo*. *J. Am. Chem. Soc.* **2020**, *142*, 10219-10227.
50. Matsumoto, H.; Silverton, S. F.; Debolt, K.; Shapiro, I. M. Superoxide-dismutase and Catalase Activities in the Growth Cartilage-relationship between Oxidoreductase Activity and Chondrocyte Maturation. *J. Bone Miner. Res.* **1991**, *6*, 569-574.
51. Takebe, G.; Yarimizu, J.; Saito, Y.; Hayashi, T.; Nakamura, H.; Yodoi, J.; Nagasawa, S.; Takahashi, K. A Comparative Study on the Hydroperoxide and Thiol Specificity of the Glutathione Peroxidase Family and Selenoprotein P. *J. Biol. Chem.* **2002**, *277*, 41254-41258.
52. Katafias, A.; Impert, O.; Kita, P. Hydrogen Peroxide as a Reductant of Hexacyanoferrate(III) in Alkaline Solutions: Kinetic Studies. *Transition Met. Chem.* **2008**, *33*, 1041-1046.
53. Baxendale, J. H. Decomposition of Hydrogen Peroxide by Catalysts in Homogeneous Aqueous Solution. *Adv. Catal.* **1952**, *4*, 31-86.
54. Wilkinson, F. *Chemical Kinetics and Reaction Mechanisms*; Van Nostrand Reinhold: New York, 1980.
55. Espenson, J. H. *Chemical Kinetics and Reaction Mechanisms*; McGraw-Hill: New York, 1995.
56. Perez-Benito, J. F. A Kinetic Study of the Cytochrome *c*-Hydrogen Peroxide Reaction. *Collect. Czech. Chem. Commun.* **2006**, *71,* 1588-1610.
57. Jordan, J.; Ewing, G. J. The Protonation of Hexacyanoferrates. *Inorg. Chem.* **1962**, *1*, 587-591.
58. Arias, C.; Mata, F.; Perez-Benito, J. F. Kinetics and Mechanism of Oxidation of Iodide Ion by the Molybdenum(VI)-Hydrogen Peroxide System. *Can. J. Chem.* **1990**, *68*, 1499-1503.
59. Mikulski, C. M.; Mattucci, L.; Weiss, L.; Karayannis, N. M. Manganese(II), Iron(II) and Nickel(II) Chloride Complexes with Monodeprotonated Anionic Guanine. *Inorg. Chim. Acta* **1985**, *107*, 147-152.
60. Fanning, J. C. The Chemical Reduction of Nitrate in Aqueous Solution. *Coord. Chem. Rev.* **2000**, *199*, 159-179.
61. Addison, C. C.; Logan, N.; Wallwork, S. C.; Garner, C. D. Structural Aspects of Co-ordinated Nitrate Groups. *Quart. Rev.* **1971**, *20*, 289-322.
62. Perez-Benito, J. F.; Prado-Diaz, P. Oxidation of Hexacyanoferrate(II) Ion by Hydrogen Peroxide: Inhibition by Polyalcohols and Related Compounds. *React. Kinet. Mech. Catal.* **2022**, *135,* 2897-2913.

63. Zheng, Z.; Wang, X.; Chen, D. Proteasome Inhibitor MG132 Enhances the Sensitivity of Human OSCC Cells to Cisplatin via a ROS/DNA Damage/p53 Axis. *Exp. Ther. Med.* **2023**, *25,* 224.
64. Perez-Benito, J. F.; Arias, C.; Amat, E. A Kinetic Study of the Reactions of Cisplatin with Biological Thiols. *New J. Chem.* **1995**, *19,* 1089-1094.
65. Marcus, R. A. On the Theory of Oxidation-Reduction Reactions Involving Electron Transfer. *J. Chem. Phys.* **1956**, *24,* 966-978.
66. Atwood, J. D.; Corrainepandolfino, M. S.; Zhen, Y. Q.; Striejewske, W. S.; Ang, P. Electron-Transfer Reactions of Metal-Carbonyl Anions. *J. Coord. Chem.* **1994**, *32,* 65-78.
67. Marcus, R. A. Reflections on Electron Transfer Theory. *J. Chem. Phys.* **2020**, *153,* 210401.
68. Perez-Benito, J. F. Some Considerations on the Fundamentals of Chemical Kinetics: Steady State, Quasi-Equilibrium, and Transition State Theory. *J. Chem. Educ.* **2017**, *94,* 1238-1246.

APPENDICES

APPENDIX 1: *Pseudo-n order plots: mathematical derivation*

When monitoring a reaction using UV-Vis spectroscopy, if the light-absorbing species is one of the reaction products [just like the yellow hexacyanoferrate(III) ion], the Lambert-Beer law can be written as:

$$A_t = \varepsilon_\lambda \, l \, (c_o - c_t) \tag{1-A}$$

where ε_λ is the molar absorption coefficient, l the optical path length, c_o and c_t being the concentrations of the limiting reactant at the beginning of the reaction and at time *t*, respectively, and where it has been considered that all the involved intermediates are present in minute concentration (in steady state), so that 1 mol of the limiting reactant yields 1 mol of the product.

Application of eq 1-A at the instant when the reaction finalizes leads to:

$$A_\infty = \varepsilon_\lambda \, l \, c_o \tag{2-A}$$

and from eqs 1-A and 2-A:

$$c_o = \frac{A_\infty}{\varepsilon_\lambda \, l} \tag{3-A}$$

$$c_t = \frac{A_\infty - A_t}{\varepsilon_\lambda \, l} \tag{4-A}$$

Now that we have the relationships between the concentrations of the limiting reactant and the absorbances measured by the spectrophotometer, it is time for us to go to the well-known integrated rate laws for the pseudo-first, pseudo-second and pseudo-*n* order reactions, being respectively:

$$\ln c_t = \ln c_o - \nu \, k_1 \, t \tag{5-A}$$

$$\frac{1}{c_t} = \frac{1}{c_o} + \nu \, k_2 \, t \tag{6-A}$$

$$\frac{1}{c_t^{n-1}} = \frac{1}{c_o^{n-1}} + (n-1) \, \nu \, k_n \, t \tag{7-A}$$

where v is the stoichiometric coefficient of the limiting reactant and k_n is the pseudo-rate constant of order n.

Finally, from eqs (3-A)-(7-A):

$$\ln (A_\infty - A_t) = \ln A_\infty - v\, k_1\, t \tag{8-A}$$

$$\frac{1}{A_\infty - A_t} = \frac{1}{A_\infty} + \frac{v\, k_2\, c_o}{A_\infty}\, t \tag{9-A}$$

$$\frac{1}{(A_\infty - A_t)^{n-1}} = \frac{1}{A_\infty{}^{n-1}} + \frac{(n-1)\, v\, k_n\, c_o^{n-1}}{A_\infty{}^{n-1}}\, t \tag{10-A}$$

that are precisely the mathematical equations used for the attempted pseudo-first (see Figure 2, left) and pseudo-second (see Figure 2, right) order plots, as well as for the pseudo-n order plots (see Figure 3), respectively.

APPENDIX 2: *Statistical treatment of experimental errors*

Both the intercept (a) and slope (b) of each experimental linear relationship were obtained by means of the following mathematical expressions derived from the method of least squares:

$$a = \frac{\sum_{i=1}^{N} x_i^2 \sum_{i=1}^{N} y_i - \sum_{i=1}^{N} x_i \sum_{i=1}^{N} x_i y_i}{N \sum_{i=1}^{N} x_i^2 - \left(\sum_{i=1}^{N} x_i\right)^2} \quad (11\text{-A})$$

$$b = \frac{N \sum_{i=1}^{N} x_i y_i - \sum_{i=1}^{N} x_i \sum_{i=1}^{N} y_i}{N \sum_{i=1}^{N} x_i^2 - \left(\sum_{i=1}^{N} x_i\right)^2} \quad (12\text{-A})$$

whereas the respective accidental (random) errors were calculated using the formulas:

$$E(a) = S_2 \sqrt{\frac{1}{N S_1} \left(\sum_{i=1}^{N} x_i^2\right)} \quad (13\text{-A})$$

$$E(b) = \frac{S_2}{\sqrt{S_1}} \quad (14\text{-A})$$

parameters S_1 and S_2 being given by:

$$S_1 = \sum_{i=1}^{N} x_i^2 - \frac{\left(\sum_{i=1}^{N} x_i\right)^2}{N} \quad (15\text{-A})$$

$$S_2 = \sqrt{\frac{1}{N-2} \left[\sum_{i=1}^{N} y_i^2 - \frac{\left(\sum_{i=1}^{N} y_i\right)^2}{N} - b \sum_{i=1}^{N} x_i y_i + \frac{b \sum_{i=1}^{N} x_i \sum_{i=1}^{N} y_i}{N}\right]} \quad (16\text{-A})$$

where x_i and y_i stand respectively for the abscissa and ordinate of each couple of data, and N is the total number of experimental points.

In this way, from the errors associated with the intercept and slope of each linear relationship it has been possible to calculate many of the experimental errors given in the present work, such as those shown in Table 1 or those associated with the activation parameters of the non-catalytic and catalytic reaction pathways.

APPENDIX 3: *Formation equilibria of the peroxomolybdate complexes*

It might be interesting to know the concentration of each one of the four complexes formed between the catalyst and the oxidant as a function of the initial concentrations of the latter, although the difficulty of the involved problem may make it look a little challenging at first sight. Six unknown variables have to be searched for and all of them, as well as the six known data required to establish the necessary equations, are compiled in Table 1-A.

Known parameters	Unknown variables
$[HMoO_4^-]_o$	$[HMoO_4^-]$
$[H_2O_2]_o$	$[H_2O_2]$
$K_{c,1}$	$[C_1]$
$K_{c,2}$	$[C_2]$
$K_{c,3}$	$[C_3]$
$K_{c,4}$	$[C_4]$

(a) $K_{c,x}$ (x = 1 – 4) stands for the equilibrium constant of formation of each peroxomolybdate(VI) complex.
(b) C_x (x = 1 – 4) stands for each peroxomolybdate(VI) complex.
(c) The magnitudes listed as unknown variables are the concentrations of the different species in the equilibrium state.

Table 1-A. Starting known parameters and searched unknown variables involved in the equilibrium problem.

The reactions of formation of the four peroxomolybdate(VI) complexes can be written as:

$$HMoO_4^- + H_2O_2 \overset{K_{c,1}}{\rightleftharpoons} H[MoO_3(O_2)]^- + H_2O \qquad (17\text{-A})$$

$$H[MoO_3(O_2)]^- + H_2O_2 \overset{K_{c,2}}{\rightleftharpoons} H[MoO_2(O_2)_2]^- + H_2O \qquad (18\text{-A})$$

$$H[MoO_2(O_2)_2]^- + H_2O_2 \overset{K_{c,3}}{\rightleftharpoons} H[MoO(O_2)_3]^- + H_2O \qquad (19\text{-A})$$

$$H[MoO(O_2)_3]^- + H_2O_2 \overset{K_{c,4}}{\rightleftharpoons} H[Mo(O_2)_4]^- + H_2O \qquad (20\text{-A})$$

The six equations that can be written to solve this mathematical problem consist of four mass action laws and two matter balances:

$$K_{c,1} = \frac{[C_1]}{[HMoO_4^-]\,[H_2O_2]} \quad (21\text{-A})$$

$$K_{c,2} = \frac{[C_2]}{[C_1]\,[H_2O_2]} \quad (22\text{-A})$$

$$K_{c,3} = \frac{[C_3]}{[C_2]\,[H_2O_2]} \quad (23\text{-A})$$

$$K_{c,4} = \frac{[C_4]}{[C_3]\,[H_2O_2]} \quad (24\text{-A})$$

$$[HMoO_4^-]_o = [HMoO_4^-] + [C_1] + [C_2] + [C_3] + [C_4] \quad (25\text{-A})$$

$$[H_2O_2]_o = [H_2O_2] + [C_1] + 2[C_2] + 3[C_3] + 4[C_4] \quad (26\text{-A})$$

where C_1, C_2, C_3 and C_4 stand for the different complexes, the subscript indicating the number of peroxo ligands, whereas eqs 25-A and 26-A are matter balances for molybdenum and the peroxo groups, respectively.

In order to easy the involved mathematics, let us consider a situation where hydrogen peroxide is in large excess with respect to the catalyst, thus eq 26-A reduces to $[H_2O_2] \approx [H_2O_2]_o$, and we have now five equations with five unknown variables. The way to handle this large set of equations is to reduce progressively the number of unknown variables (and correspondingly of equations) step by step, one at a time, leading to:

$$[C_1] = \frac{[C_4]}{K_{c,2}\,K_{c,3}\,K_{c,4}\,[H_2O_2]_o^3} \quad (27\text{-A})$$

$$[C_2] = \frac{[C_4]}{K_{c,3}\,K_{c,4}\,[H_2O_2]_o^2} \quad (28\text{-A})$$

$$[C_3] = \frac{[C_4]}{K_{c,4}\,[H_2O_2]_o} \quad (29\text{-A})$$

the concentration of the tetraperoxomolybdate(VI) complex being:

$$[C_4] = \frac{f_4\,[HMoO_4^-]_o\,[H_2O_2]_o^4}{1 + f_1\,[H_2O_2]_o + f_2\,[H_2O_2]_o^2 + f_3\,[H_2O_2]_o^3 + f_4\,[H_2O_2]_o^4} \quad (30\text{-A})$$

where:

$$f_1 = K_{c,1} \quad (31\text{-A})$$

$$f_2 = K_{c,1}\,K_{c,2} \quad (32\text{-A})$$

$$f_3 = K_{c,1}\,K_{c,2}\,K_{c,3} \quad (33\text{-A})$$

$$f_4 = K_{c,1}\,K_{c,2}\,K_{c,3}\,K_{c,4} \quad (34\text{-A})$$

Therefore, the initial catalytic reaction pathway has been finally split into eight pathways, in each of them reacting one of the four peroxo complexes either with the anhydrous form or the hydrated form of hexacyanoferrate(II) ion, the total initial rate of the catalytic paths being given by the sum of the eight partial rates. Thus, with the help of eqs 54 and 55 we can write:

$$v_{o,c} = \sum_{x=1}^{4} \frac{K_{7,x}\,k_{S,x}\,[HMo^{VI}O_{4-x}(O_2)_x^-]_o\,[H^+]_o}{2\,(1 + K_{7,x}\,[H^+]_o)} \quad (35\text{-A})$$

where:

$$k_{S,x} = k_{8,x}\,[Fe^{II}(CN)_6^{4-}]_o + K_1^{1/2}\,k_{9,x}\,[Fe^{II}(CN)_6^{4-}]_o^{1/2} \quad (36\text{-A})$$

Equation 36-A is consistent with the apparent kinetic order of iron(II) in the catalytic reaction pathway intermediary between 0.5 and 1 (see Table 1). Moreover, eqs (27-A)-(30-A) and 35-A are also consistent with the first-order dependence on the catalyst initial concentration (Figure

6), as well as with the fast increase of the pseudo-first order rate constant with the initial concentration of hydrogen peroxide and with the observed posterior plateau (Figure 8, right), the initial rate corresponding to the latter being given by:

$$\lim_{[H_2O_2]_o \to \infty} v_{o,c} = \frac{K_{7,4}\, k_{S,4}\, [HMoO_4^-]_o\, [H^+]_o}{2\,(1 + K_{7,4}\, [H^+]_o)} \qquad (37\text{-A})$$

and the associated pseudo-first order rate constant:

$$\lim_{[H_2O_2]_o \to \infty} k_c = \frac{K_{7,4}\, k_{S,4}\, [H^+]_o}{2\,(1 + K_{7,4}\, [H^+]_o)} \qquad (38\text{-A})$$

since, when the initial concentration of hydrogen peroxide is high enough, almost all the molybdenum(VI) is in the tetraperoxo form (x = 4).